nature microbiology

ARTICLES

https://doi.org/10.1038/s41564-019-0649-5

Endogenous murine microbiota member *Faecalibaculum rodentium* and its human homologue protect from intestinal tumour growth

Elena Zagato[1,18,20], Chiara Pozzi[2,20], Alice Bertocchi[2], Tiziana Schioppa[3], Fabiana Saccheri[1], Silvia Guglietta[1,19], Bruno Fosso[4], Laura Melocchi[5,6], Giulia Nizzoli[7], Jacopo Troisi[8,9,10], Marinella Marzano[4], Bianca Oresta[2], Ilaria Spadoni[11], Koji Atarashi[12,13], Sara Carloni[11], Stefania Arioli[14], Giulia Fornasa[2], Francesco Asnicar[15], Nicola Segata[15], Simone Guglielmetti[14], Kenya Honda[12,13], Graziano Pesole[4,16], William Vermi[5,17], Giuseppe Penna[2] and Maria Rescigno[2,11]*

The microbiota has been shown to promote intestinal tumourigenesis, but a possible anti-tumourigenic effect has also been postulated. Here, we demonstrate that changes in the microbiota and mucus composition are concomitant with tumourigenesis. We identified two anti-tumourigenic strains of the microbiota—*Faecalibaculum rodentium* and its human homologue, *Holdemanella biformis*—that are strongly under-represented during tumourigenesis. Reconstitution of Apc$^{Min/+}$ or azoxymethane- and dextran sulfate sodium-treated mice with an isolate of *F. rodentium* (*F.* PB1) or its metabolic products reduced tumour growth. Both *F.* PB1 and *H. biformis* produced short-chain fatty acids that contributed to control protein acetylation and tumour cell proliferation by inhibiting calcineurin and NFATc3 activation in mouse and human settings. We have thus identified endogenous anti-tumourigenic bacterial strains with strong diagnostic, therapeutic and translational potential.

Colorectal cancer (CRC) is a multifactorial disorder influenced by genetic, environmental and lifestyle factors, including the deregulation of the microbiota[1]. A decrease in *Clostridium* and *Bacteroides* and an increase in *Fusobacterium*[2,3] has been reported in CRC as well as in association with recurrence[4]. The role of bacteria in tumourigenesis has been extensively demonstrated in spontaneous mouse models of tumourigenesis, such as Apc$^{Min/+}$ mice, which carry a mutation in the *adenomatous polyposis coli* (*APC*) gene, which is mutated in more than 80% of sporadic CRCs[5]. Microbiota-derived signals drive ERK phosphorylation and increased stability of the oncogene *Myc*, or trigger the c-Jun/JNK and STAT3 signalling pathways driving cell proliferation and accumulation of suppressive immune cells within the tumour[6] or the exacerbation of the inflammatory response[7]. Enterotoxigenic *Bacteroides fragilis*[8] and colibactin-producing *Escherichia coli*[9] exert their pro-tumourigenic effect through bacterial toxins. On the other hand, in an inflammation-induced model of colitis-associated CRC, germ-free mice develop significantly more and larger tumours after treatment with azoxymethane (AOM) and dextran sulfate sodium (DSS) compared with specific-pathogen-free mice[9,10]. After faecal-microbiota transplantation, germ-free mice treated with AOM and DSS develop more tumours than healthy mice if transplanted with faecal microbiota from CRC patients but it is not clear whether this is due to an increase in tumour-promoting bacteria, a decrease in anti-tumourigenic bacteria or both[11]. Furthermore, a diet rich in fibres can protect against tumour development in a microbiota-dependent manner[12]. Thus, although most studies have concentrated on identifying tumour-promoting bacteria, the role and identification of endogenous anti-tumourigenic microbiota remains elusive.

Here, we identified an endogenous strain of the mouse microbiota (*Faecalibaculum rodentium* isolate PB1) and its human counterpart *Holdemanella biformis* belonging to the Erysipelotrichaceae family, which are lost during the early phases of tumourigenesis and block tumour-cell proliferation by reducing activation of nuclear factor of activated T cells, cytoplasmic 3 (NFATc3) and calcineurin.

Results

***F. rodentium* is under-represented during the early phases of tumourigenesis**. We followed the changes in microbiota composition in a longitudinal study in cohorts of Apc$^{Min/+}$ mice and

[1]Department of Experimental Oncology, European Institute of Oncology IRCCS, Milan, Italy. [2]Humanitas Clinical and Research Center, IRCCS, Milan, Italy. [3]Department of Molecular and Translational Medicine, University of Brescia, Brescia, Italy. [4]Institute of Biomembranes, Bioenergetics and Molecular Biotechnologies, Consiglio Nazionale delle Ricerche, Bari, Italy. [5]Section of Pathology, Department of Molecular and Translational Medicine, University of Brescia, Brescia, Italy. [6]Pathology Department, Fondazione Poliambulanza Hospital, Brescia, Italy. [7]Gastroenterology and Endoscopy Unit, Fondazione IRCCS Cà Granda, Ospedale Maggiore Policlinico, Milan, Italy. [8]Department of Medicine, Surgery and Dentistry, Scuola Medica Salernitana, University of Salerno, Baronissi, SA, Italy. [9]Theoreo Srl, Montecorvino Pugliano, Italy. [10]European Biomedical Research Institute of Salerno, Salerno, Italy. [11]Department of Biomedical Sciences, Humanitas University, Milan, Italy. [12]RIKEN Center for Integrative Medical Sciences, Tsurumi-ku, Yokohama, Japan. [13]Department of Microbiology and Immunology, Keio University School of Medicine, Tokyo, Japan. [14]Division of Food Microbiology and Bioprocesses and Department of Food, Environmental and Nutritional Sciences, Università degli Studi di Milano, Milan, Italy. [15]CIBIO Department, University of Trento, Trento, Italy. [16]Department of Biosciences, Biotechnology and Biopharmaceutics, University of Bari, Bari, Italy. [17]Department of Pathology and Immunology, Washington University, Saint Louis, MO, USA. [18]Present address: Institute of Oncology Research, Università della Svizzera italiana, Bellinzona, Switzerland. [19]Present address: Department of Microbiology and Immunology, Hollings Cancer Center, Medical University of South Carolina, Charleston, SC, USA. [20]These authors contributed equally: Elena Zagato, Chiara Pozzi. *e-mail: maria.rescigno@hunimed.eu

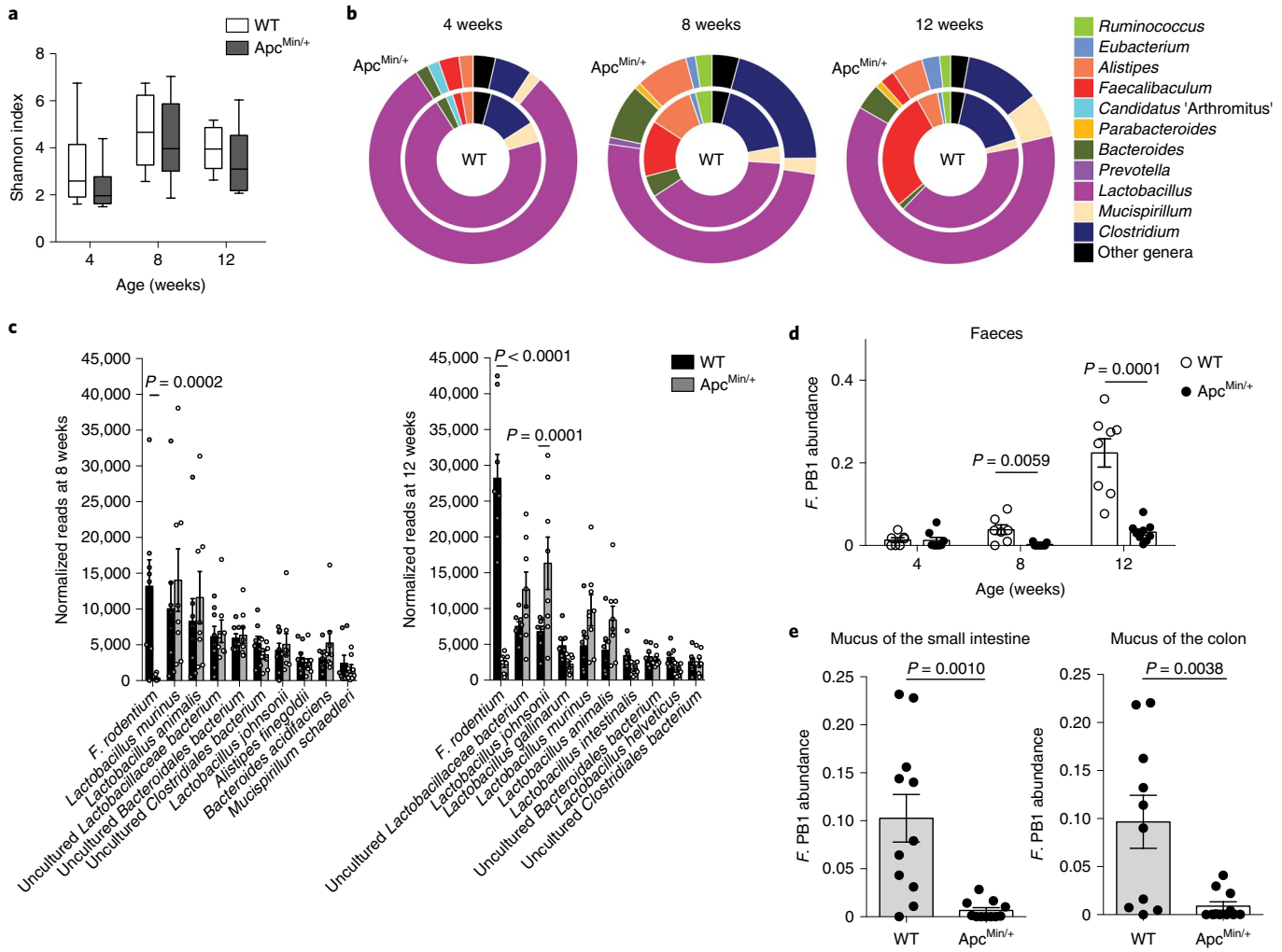

Fig. 1 | *F. rodentium* is under-represented during the early phases of tumour development. a–**c**,16S rRNA gene profiling of the faecal microbiota of WT and Apc$^{Min/+}$ mice at the age of 4, 8 and 12 weeks ($n=8$ mice per group). **a**, Shannon diversity index. The box plots show the interquartile range, the horizontal lines show the median values and the whiskers indicate the minimum-to-maximum range. **b**, Genus abundance in WT (inner pie) and Apc$^{Min/+}$ (outer pie) mice. Genera with a relative abundance >1% in at least one of the tested conditions are shown, otherwise they are collapsed into the 'Other genera' section. *P* values discussed in the main text were calculated using a two-tailed unpaired Mann–Whitney *U*-test. **c**, Relative abundance of the ten-most abundant species in faecal bacterial DNA isolated from eight- (left) and 12-week-old (right) WT and Apc$^{Min/+}$ mice. Abundance is shown as the normalized number of assigned sequences in the 16S rRNA sequencing. *P* values were determined using a two-way analysis of variance (ANOVA) with Bonferroni's post-hoc test. **d**,**e**, Abundance of *F.* PB1, determined by qPCR, normalized to pan-bacterial primers targeting the 16S rRNA gene (UNI 16S) in bacterial DNA extracted from faeces (**d**; $n=8$ mice per group) and mucus from the small intestine (**e**, left) and colon (**e**, right; $n=11$ mice per group) of WT and Apc$^{Min/+}$ mice. *P* values were determined using multiple *t*-tests corrected for multiple comparisons using the Holm–Sidak method to compare *F.* PB1 abundance between groups at each time point (**d**) or using a two-tailed unpaired Student's *t*-test (**e**). Data are from two independent experiments and represented as the mean ± s.e.m.

age- and sex-matched C57BL/6 wild-type (WT) littermates born from the same mothers. Bacterial DNA was extracted from their faeces at 4, 8 and 12 weeks. As shown in Fig. 1a and Extended Data Fig. 1a, we did not observe any change in the Shannon, Chao1 and Simpson-diversity indexes among the two groups at any age, whereas we observed differences in genus abundance at 8 and 12 weeks (Fig. 1b). We observed a quantitative contraction of the paired-end reads ascribed to the genus *Faecalibaculum* as early as 8 weeks ($P < 0.01$) when tumours started developing (Extended Data Fig. 1b), which became even more pronounced at 12 weeks ($P<0.0005$) in Apc$^{Min/+}$ mice compared with their WT littermates. Moreover, we detected an expansion of paired-end reads associated with *Lactobacillus* ($P=0.04$), *Parabacteroides* ($P=0.03$) and *Bacteroides* ($P=0.016$) in Apc$^{Min/+}$ mice compared with WT mice but only at 12 weeks (Fig. 1b).

Among the ten-most abundantly represented taxonomic units of WT mice, we found that only the reads ascribed to *F. rodentium*[13] were strongly and significantly under-represented in Apc$^{Min/+}$ mice compared with WT mice ($P<0.001$). This taxon was not expanded in eight-week-old Apc$^{Min/+}$ mice, coincident with the initiation of tumour development (Fig. 1c and Extended Data Fig. 1c). These data were confirmed by quantitative PCR (qPCR; Fig. 1d). We then isolated and entirely sequenced a strain from WT mice belonging to this taxon and found that it is the only representative of *F. rodentium* in our WT mouse colony (Fig. 1c, not shown). The previously uncharacterized *F.* PB1 isolate was associated with the mucus of the small and large intestines but was drastically reduced in the mucus from Apc$^{Min/+}$ mice (Fig. 1e). We have thus identified a strain of *F. rodentium* that is normally highly abundant in WT mice and is strongly under-represented in Apc$^{Min/+}$ mice early in tumourigenesis.

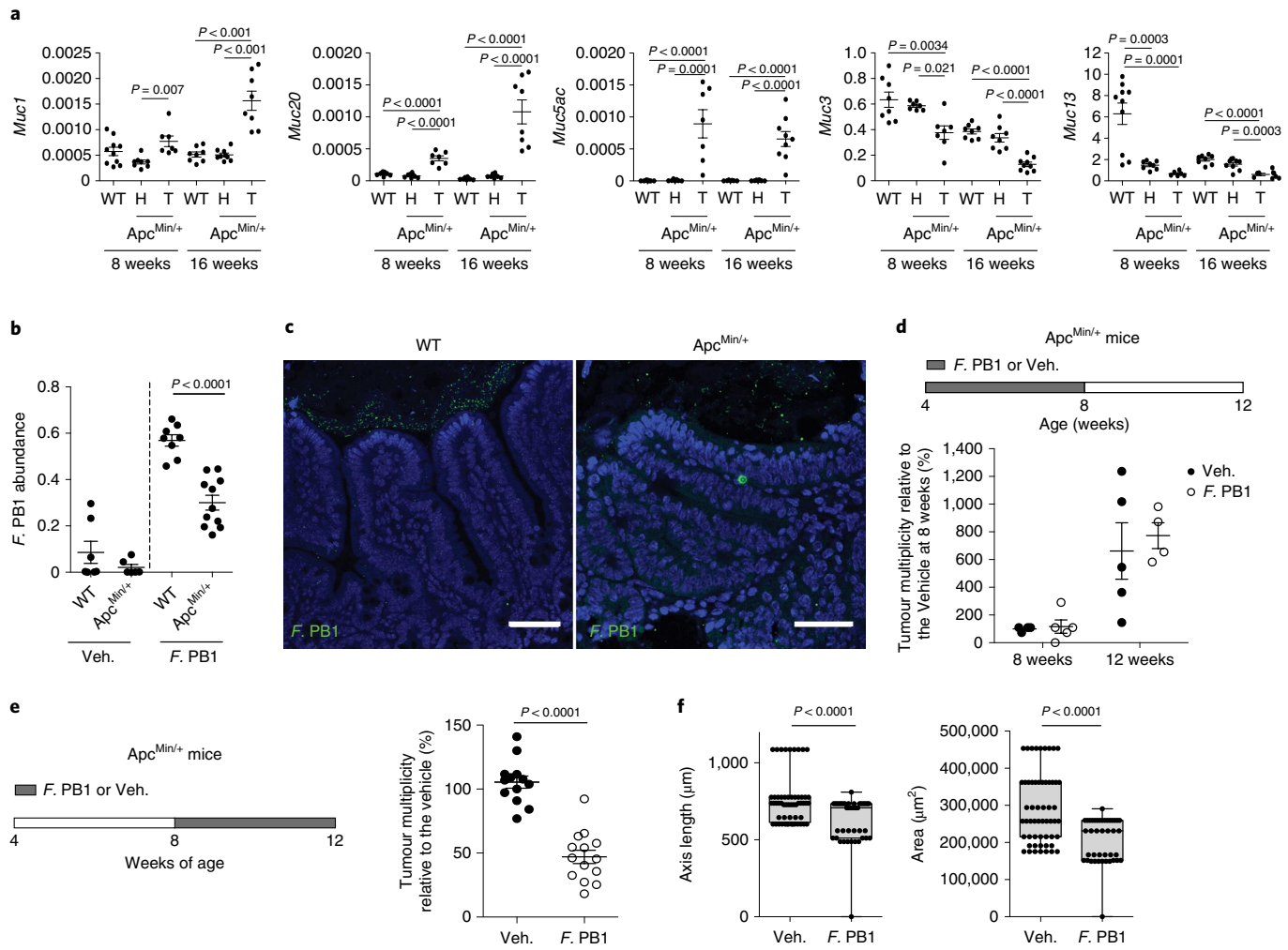

Fig. 2 | *F.* PB1 loss coincides with mucus changes and reduces tumour growth when reintroduced. a, Mucin expression in the ileal tissue of WT mice and healthy (H) and tumour (T) tissue of Apc$^{Min/+}$ mice at the age of 8 and 16 weeks was determined using qPCR. The expression levels were normalized to the reference gene *Rpl32*. Data are from two independent experiments (8 weeks, $n=10$ (WT), 8 (H) and 7 (T) mice; 16 weeks, $n=8$ (WT) and 9 (H and T) mice). *P* values were determined using a one-way ANOVA with Bonferroni's post-hoc test to compare expression levels at the same time point. **b**,**c**, *F.* PB1 administration experiments in WT and Apc$^{Min/+}$ mice pretreated with an antibiotic cocktail. **b**, *F.* PB1 abundance normalized to pan-bacterial primers targeting the 16S rRNA gene (UNI 16S) in bacterial DNA extracted from ileal mucus, determined using qPCR. Data are from two independent experiments (WT, $n=7$ (vehicle) and 10 (*F.* PB1) mice; Apc$^{Min/+}$, $n=6$ (vehicle) and 11 (*F.* PB1) mice). *P* values were determined using a two-tailed unpaired Mann–Whitney *U*-test. **c**, Representative images of fluorescence in situ hybridization of *F.* PB1 on the mucosal surface of an Apc$^{Min/+}$ ileum polyp (right) and normal WT (left) ileum. Nuclei have been stained with DAPI (blue). Scale bars, 50 µm; images were obtained at ×40 magnification; $n=3$ mice per group. **d**, Four-week-old Apc$^{Min/+}$ mice were treated with vehicle or *F.* PB1 until they were 8 weeks old (top). At 12 weeks, tumour multiplicity in the small intestine was assessed ($n=5$ mice per group). Significance was determined by multiple *t*-tests corrected for multiple comparisons using the Holm–Sidak method to compare tumour multiplicity between groups at each time point. **e**,**f**, Apc$^{Min/+}$ mice received vehicle or *F.* PB1 from week 8 to 12 (**e**, left). Two independent experiments were performed with consistent results. **e**, Tumour multiplicity in the small intestine normalized to vehicle-treated Apc$^{Min/+}$ mice at the age of 12 weeks (right). Data are from two independent experiments ($n=14$ mice per group). **f**, Area (right) and maximum diameter (axis length; left) of ileal dysplastic lesions normalized to the total number of lesions per mouse. Data are from one representative experiment ($n=7$ mice per group). The box plots show the interquartile range, the horizontal lines show the median values and the whiskers indicate the minimum-to-maximum range. *P* values were determined using a two-tailed unpaired Student's *t*-test (**e**) and two-tailed unpaired Mann–Whitney *U*-test (**f**). **a**,**b**,**d**–**f**, Data are represented as the mean ± s.e.m. Veh., vehicle.

***F.* PB1 loss coincides with mucus changes and protects from tumour development**. The mucus layer serves as a niche for the intestinal microbiota[14], and changes in its composition may influence the microbiota profile. During tumourigenesis, epithelial cell transformations could lead to modification in the production of mucins—the major components of mucus—resulting in a non-permissive environment for *F.* PB1. As shown in Fig. 2a, we observed that, similarly to human CRC (hCRC), mucin *Muc1* and *Muc20* (ref. [15]) were overexpressed, whereas *Muc5ac* was aberrantly expressed in tumours, as it is not normally expressed in the lower gastrointestinal tract[16]. We found that *Muc3* and *Muc13* were downregulated; the latter also occurred in the non-tumour region of eight-week-old Apc$^{Min/+}$ mice, suggesting that this may be an early event in tumourigenesis. We confirmed the downregulation of Muc13 protein in both tumour and non-tumour regions of Apc$^{Min/+}$ mice compared with WT mice; however, in contrast to the RNA data, Muc1 and Muc20 were downregulated in gut tissues (Extended Data Fig. 2a). This may be due to increased secretion,

as Muc1 was higher in the mucus of $Apc^{Min/+}$ tumours (Extended Data Fig. 2b).

We next tested whether *F.* PB1 was capable of colonizing $Apc^{Min/+}$ mice. We treated WT and $Apc^{Min/+}$ mice with antibiotics to eliminate competing microorganisms and administered *F.* PB1 by gavage. As shown in Fig. 2b, *F.* PB1 abundance was lower in the ileal mucus of $Apc^{Min/+}$ mice than WT mice at 48 h, suggesting that the $Apc^{Min/+}$ gut is unfavourable for *F.* PB1 colonization. This was confirmed by fluorescence-in-situ-hybridization analysis (Fig. 2c). Thus, to evaluate a possible role of *F.* PB1 in tumour protection, we administered it by gavage every other day to ensure appreciable levels throughout the experiment. We treated the $Apc^{Min/+}$ and WT littermates with *F.* PB1 either before or during tumour development. We observed that the administration of *F.* PB1 from week 4 to 8 did not affect tumour development (Fig. 2d). However, administration of *F.* PB1 from week 8 to 12 (that is, when the bacterium was not enriched in $Apc^{Min/+}$ mice) resulted in a clear reduction in the tumour numbers and dimensions (Fig. 2e,f). The reduction in tumour multiplicity observed macroscopically was no longer statistically significant when the number of lesions were microscopically analysed (Extended Data Fig. 2c), indicating that some small lesions were not visible to the eye and that *F.* PB1 probably affects tumour growth instead of initiation.

These results suggest that the modification in mucus composition creates an unfavourable environment for *F.* PB1 colonization. Administration of *F.* PB1 has an antitumour effect only when tumours have already started developing.

***F.* PB1 affects tumour cell proliferation without a major impact on adaptive immune cells**. The antitumour activity of *F.* PB1 may depend on the immune system. We thus assessed the capacity of *F.* PB1 to activate an immune response in the absence of confounding microbiota, through monocolonization of germ-free mice. As shown in Extended Data Fig. 3, *F.* PB1 did not significantly impact immune-cell development. The number of FoxP3+ regulatory T cells in the small intestine lamina propria was unaffected by *F.* PB1 and only slightly changed in the large intestine (Extended Data Fig. 3a); in addition, no effects on IL17- or IFNγ-producing $CD4^+$ T cells were observed at either location (Extended Data Fig. 3b,c). We then analysed the effect of *F.* PB1 in $Apc^{Min/+}$ mice. We could not detect any difference in the frequencies of any of the tested $CD4^+$ T cell populations ($FoxP3^+$ regulatory T, Th1 and Th17 cells) in specific-pathogen-free $Apc^{Min/+}$ mice that were administered *F.* PB1. However, we observed a trend towards a reduction in their absolute numbers (Fig. 3a and Extended Data Fig. 3d,e). We then analysed the innate immune cell components, and found no difference in neutrophil frequencies and counts in the lamina propria of the small intestine, whereas we observed a reduction in all of the mononuclear phagocytes in $Apc^{Min/+}$ mice administered with *F.* PB1 (Extended Data Fig. 3f,g).

Consistent with our previous data, we observed a higher, albeit non-significant, frequency of circulating $Ly6G^+CD11b^+$ neutrophils in 12-week-old $Apc^{Min/+}$ mice compared with their WT littermates[17] regardless of *F.* PB1 treatment. In contrast, treatment with *F.* PB1 resulted in the reduction of circulating $Ly6C^{high}CD11b^+$ inflammatory monocytes in both WT and $Apc^{Min/+}$ mice (Fig. 3b and Extended Data Fig. 3h). Hence, the reduction of gut inflammatory monocytes may be due to a reduction of circulating monocytes during *F.* PB1 treatment.

We then evaluated whether *F.* PB1 was acting directly on tumour cell growth. We administered *F.* PB1 to eight-week-old mice and then analysed tumour growth two weeks later. Treatment with *F.* PB1 induced a reduction in tumour number (macroscopic evaluation; Fig. 3c), tumour size (Fig. 3d), tumour cell proliferation (Fig. 3e,f) and rectal bleeding (Fig. 3g).

We next analysed whether *F.* PB1 administration had changed the microbiota composition and its metabolic output. Bacterial DNA was extracted from the faeces of $Apc^{Min/+}$ mice treated with or without *F.* PB1 and the 16S ribosomal RNA gene profiling data were analysed. We observed an increase in short-chain fatty acid (SCFA)-producing bacteria in mice treated with *F.* PB1, particularly *Butyricimonas* (butyric acid-producing bacteria[18]; Extended Data Fig. 4a). As these and the other SCFA-producing bacteria were not reduced in the initial assessment of microbiota in untreated $Apc^{Min/+}$ versus WT mice during tumour development, it is unlikely that they have an impact on tumourigenesis.

It has been reported that $Apc^{Min/+}$ mice with a *niacr1* (GPR109A, the receptor for butyrate) gene deletion are more susceptible to tumour development via a mechanism that depends on the microbiota[19]. We thus evaluated whether *F.* PB1 administration may affect the faecal level of SCFAs. We detected an increase in SCFAs (propionate, butyrate and acetate) and a reduction in lactate in the faecal content of mice treated with *F.* PB1 at the age of 12 weeks compared with 8 weeks (Fig. 3h). No significant differences in the levels of succinate and isovalerate were observed between treated and untreated mice, whereas a slight increase in valerate was observed in treated mice (Extended Data Fig. 4b).

These results suggest that *F.* PB1 affects tumour cell proliferation alone or in cooperation with other bacteria, probably through the release of SCFAs.

***F.* PB1 releases SCFAs that have anti-proliferative activities**. Butyrate has been described to have histone deacetylase (HDAC) inhibitory activity[20], which affects cell proliferation. In contrast to normal epithelial cells, CRC cells do not use butyrate for their growth and its concentration accumulates, acting as an HDAC inhibitor (HDACi)[21,22]. We carried out a dose-dependent response assay on four different mouse intestinal tumour cell lines (APC, CT26, MC-38 and CMT-93) and found that maximal cell growth inhibition, without cell viability being compromised, occurred at 1–2 mM butyrate and at much higher doses of acetate and propionate (2,5–50 mM). We found that the combination of SCFAs had an additive effect on the inhibition of the proliferation of all tested cell lines (Fig. 4a).

We then assessed whether *F.* PB1 itself was capable of synthesizing SCFAs in vitro. *F.* PB1 grown in strictly anaerobic conditions was very efficient at producing both butyrate and lactate (Fig. 4b). Interestingly, the concentration of butyrate (1 mM) was very similar to the one able to inhibit cell proliferation as indentified in the dose-dependant response assay (Fig. 4a), whereas that of acetate or propionate was extremely low (250–5,000× lower than the effective concentration on cell lines in vitro). Next, we evaluated whether the *F.* PB1 spent medium (SUP), containing SCFAs, had anti-proliferative activity. As shown in Fig. 4c, the addition of SUP drastically inhibited tumour cell proliferation without affecting tumour cell viability (not shown), suggesting that *F.* PB1 releases metabolites that interfere with cell proliferation.

A recent report has shown that tumourigenesis in hCRC and $Apc^{Min/+}$ mice is dependent on the calcineurin-mediated activation of the NFATc3 transcription factor, which is important for cell proliferation[23]. Because the HDACi panobinostat can induce calcineurin degradation in multiple myeloma cells[24], we assessed whether the SCFAs produced by *F.* PB1 could act as HDAC inhibitors and therefore affect calcineurin and NFATc3 activation. This would explain why the administration of *F.* PB1 or its spent medium could inhibit tumour cell proliferation. Treatment with *F.* PB1 SUP (Fig. 4d) or the combination of SCFAs (Extended Data Fig. 5a) drastically increased the acetylation of histone H3 (H3K27ac), thereby confirming its HDACi activity. This correlated with the downregulation of calcineurin (PP2B-A) and NFATc3 activation in CRC cell lines (Fig. 4d and Extended Data Fig. 5b).

Short-chain fatty acids are volatile and can be extracted through evaporation. Thus, we compared the effect of the untreated *F.* PB1

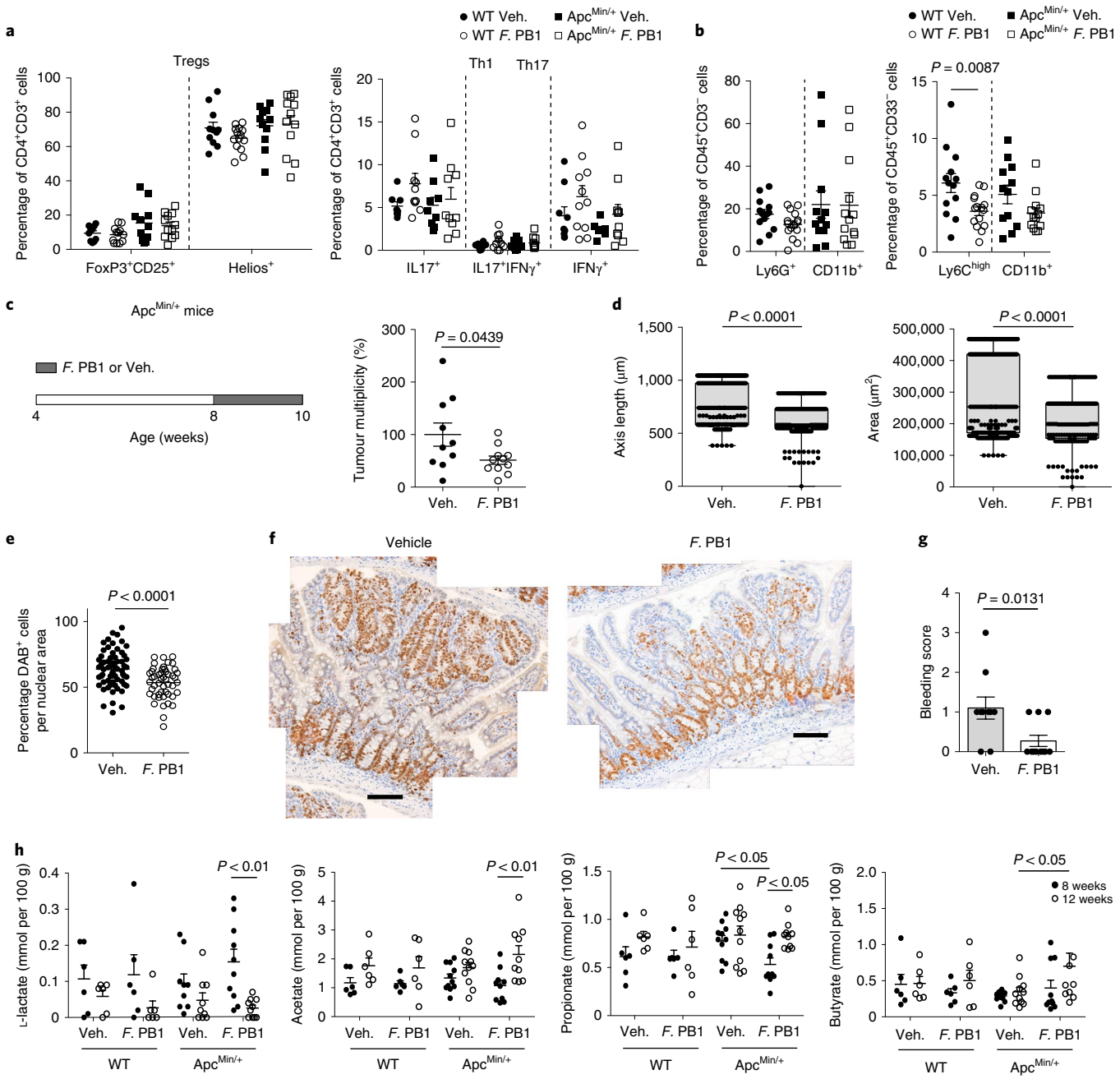

Fig. 3 | *F.* PB1 reduces tumour cell proliferation without a major impact on immune cells. a,**b**, Wild-type and Apc$^{Min/+}$ mice were treated with vehicle (Veh.) or *F.* PB1 from week 8 to 12. **a**, Flow cytometric analysis of regulatory T (Tregs), Th1 and Th17 cell populations in the lamina propria of the small intestine. FoxP3$^+$ and CD25$^+$ cells were gated on live CD45$^+$CD3$^+$CD4$^+$ cells; Helios$^+$ cells were gated on FoxP3$^+$CD25$^+$ cells (left; $n=12$ (WT Veh. and Apc$^{Min/+}$ *F.* PB1), 14 (WT *F.* PB1) and 11 (Apc$^{Min/+}$ Veh.) mice). IL17$^+$, IFNγ$^+$ and IL17$^+$IFNγ$^+$ cells were gated on live CD45$^+$CD3$^+$CD4$^+$ cells (right; $n=9$ (WT Veh. and Apc$^{Min/+}$ Veh.), 11 (WT *F.* PB1) and 10 (Apc$^{Min/+}$ *F.* PB1) mice). **b**, Flow cytometric analysis of peripheral blood cells. Percentages are relative to the CD45$^+$CD3$^-$ population ($n=13$ (WT Veh. and Apc$^{Min/+}$ *F.* PB1), 15 (WT *F.* PB1) and 12 (Apc$^{Min/+}$ Veh.) mice). **c**–**g**, Apc$^{Min/+}$ mice received vehicle or *F.* PB1 from week 8 to 10 (**c**, left). Data are from two independent experiments. **c**, Tumour multiplicity in the small intestine normalized to vehicle-treated Apc$^{Min/+}$ mice ($n=10$ (Veh.) and 11 (*F.* PB1) mice). **d**, Area (right) and maximum diameter (left) of ileal dysplastic lesions ($n=265$ (Veh.) and 150 (*F.* PB1) lesions) normalized to the total number of lesions per mouse. The box plots show the interquartile range, the horizontal lines show the median values and the whiskers indicate the minimum-to-maximum range ($n=10$ (Veh.) and 11 (*F.* PB1) mice). **e**, Percentage of nuclear Ki67$^+$ cells in the polyps of mice treated with vehicle and *F.* PB1 ($n=4$ mice per group). **f**, Representative images of nuclear Ki67 staining in the polyps of vehicle- (left) and *F.* PB1-treated mice (right; $n=4$ mice per group). Scale bars, 100 μm. **g**, Bleeding score of vehicle- and *F.* PB1-treated mice ($n=10$ (Veh.) and 11 (*F.* PB1) mice). **h**, Faecal concentrations of L-lactate, acetate, propionate and butyrate in WT and Apc$^{Min/+}$ mice treated with vehicle or *F.* PB1 from 8 to 12 weeks, detected by ultra-performance liquid chromatography with high-resolution mass spectrometry (UPLC–HR–MS; $n=6$ (WT Veh. and WT *F.* PB1), 11 (Apc$^{Min/+}$ Veh.) and 10 (Apc$^{Min/+}$ *F.* PB1) mice). **a**–**d**,**g**,**h**, Data from two independent experiments are represented as the mean ± s.e.m. *P* values were determined using a one-way ANOVA with Bonferroni's post-hoc test for multiple comparisons (**a**), two-tailed unpaired Student's *t*-test (**b**,**c**,**e**,**g**), two-tailed unpaired Mann–Whitney *U*-test (**d**) or two-way ANOVA with Bonferroni's post-hoc test for multiple comparisons (**h**).

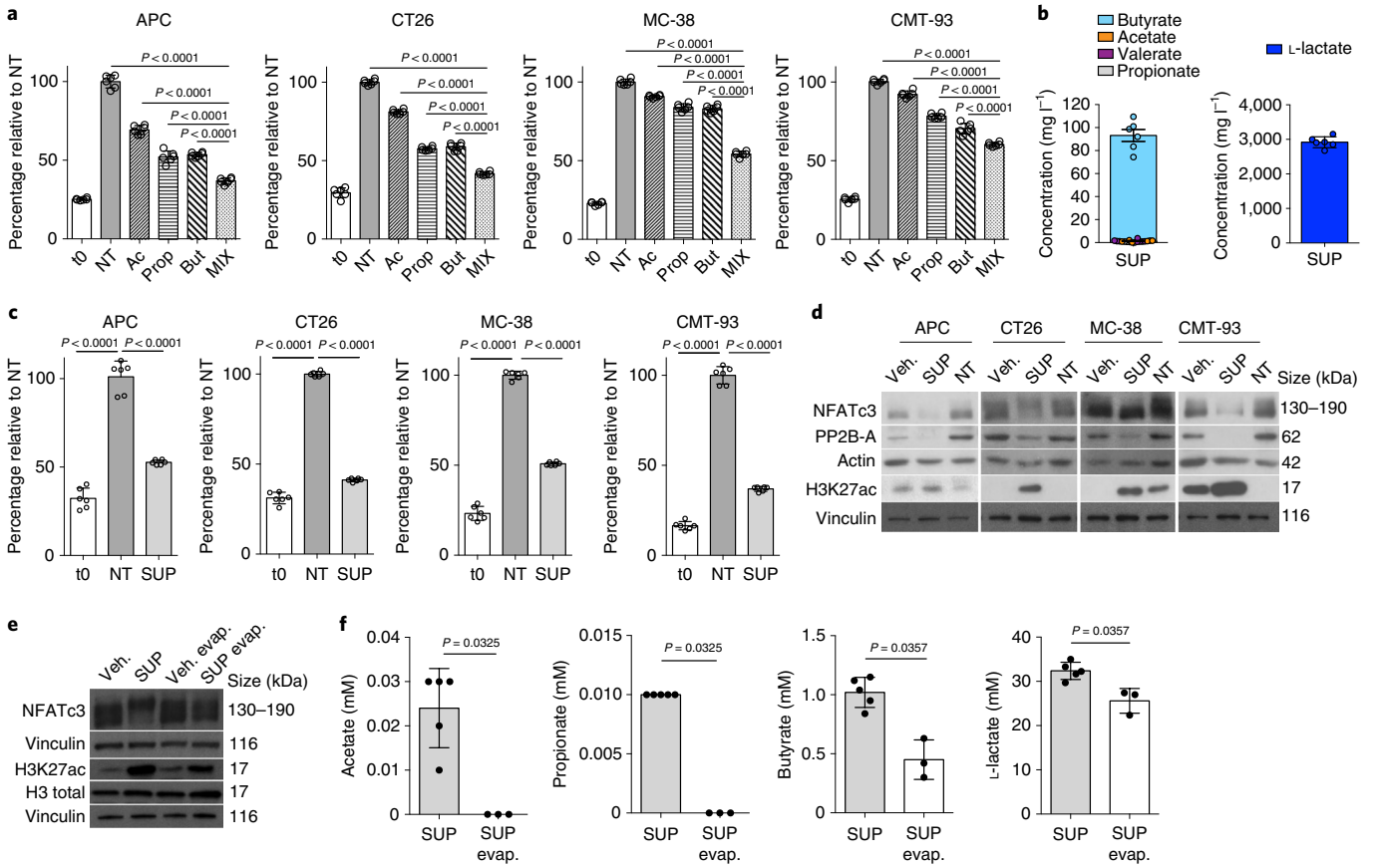

Fig. 4 | *F.* PB1 releases SCFAs that have anti-proliferative activities. a,**c**, Cell proliferation assays on mouse CRC cell lines treated or not (NT) with acetate (Ac), propionate (Prop) and butyrate (But) alone and in combination (MIX; **a**), or with *F.* PB1 SUP (**c**). t0, signal from cells at the time of stimulation. Two independent experiments were performed with consistent results. Data are from one representative experiment ($n = 6$ biologically independent samples). *P* values were determined using a one-way ANOVA with Bonferroni's post-hoc test. **b**, Levels of L-lactate and SCFAs in *F.* PB1 SUP, determined using UPLC–HR–MS. Data are from six independent experiments. **d**, Representative western blots from two or three independent experiments showing the effect of treatment with or without (NT) *F.* PB1 SUP or unfermented (Veh.) broth on H3K27 acetylation (H3K27ac), and PP2B-A and NFATc3 expression in mouse cell lines. Vinculin and actin were used as loading controls. The densitometric analysis is reported in Extended Data Fig. 5b. **e**,**f**, In vitro stimulation of CT26 cells with *F.* PB1 SUP that was either untreated or depleted of SCFAs by evaporation (SUP evap.). Untreated and unfermented (Veh.) or evaporated (Veh. evap.) broths were used as controls. **e**, Representative western blots from two independent experiments showing the effect of SUP and SUP evap. on H3K27ac and NFATc3 expression. Vinculin was used as a loading control. The densitometric analysis is reported in Extended Data Fig. 5c. **f**, Levels of SCFAs and L-lactate quantified using UPLC–HR–MS ($n = 3$ (SUP evap.) or 6 (SUP) biologically independent experiments). *P* values were determined using a two-tailed unpaired Mann–Whitney *U*-test. **a**–**c**,**f**, Data are presented as the mean ± s.d.

SUP with *F.* PB1 SUP subjected to evaporation to deplete the SCFAs. Although there was a minor effect of SUP evaporation on the concentration of lactate, the evaporated SUP was strongly impaired in inducing H3 acetylation and NFATc3 downregulation, which suggests that lactate was not involved in this process (Fig. 4e,f and Extended Data Fig. 5c). In contrast, there was very little acetate and propionate in the evaporated SUP, whereas the concentration of butyrate was halved. The residual effect on H3 acetylation and NFATc3 downregulation could thus be due to the left-over butyrate still present in the supernatant after evaporation (Fig. 4f) or to other metabolites that were unaffected by evaporation. Hence, *F.* PB1 releases metabolites, including SCFAs, that can impact tumour cell proliferation by inhibiting HDACs and thus block NFATc3 and calcineurin activation.

The *F.* PB1 metabolic products have an anti-proliferative activity in vivo and this is independent of the microbiota. We next evaluated whether the *F.* PB1 SUP had anti-tumourigenic activity in vivo. The *F.* PB1 SUP did not statistically affect tumour multiplicity, but the size of the tumour lesions was significantly reduced (Fig. 5a,b and Extended Data Fig. 6a). We then pre-treated 11-week-old $Apc^{Min/+}$ mice (that had already developed tumours) with antibiotics to affect the microbiota but not tumour growth, and then administered SUP in the presence of antibiotics. We observed an even greater reduction in the dimensions of the tumour lesions, which indicated that the spent medium had an anti-proliferative activity in vivo that was independent of the microbiota (Fig. 5c,d and Extended Data Fig. 6b). Furthermore, the SUP reduced NFATc3 activation and induced histone H3 acetylation in dysplastic lesions, again in a microbiota-independent fashion (Fig. 5e). These data suggest that the metabolic products of *F.* PB1 have a direct effect on tumour growth and affect NFATc3 activation.

We then evaluated whether butyrate was sufficient to mediate the anti-proliferative response. We administered 1 mM sodium butyrate (the same concentration found in the SUP of *F.* PB1) to $Apc^{Min/+}$ mice treated with antibiotics to avoid the possibility of butyrate being used up by the indigenous microbiota. As shown in Fig. 5f,g, butyrate had a very similar anti-proliferative activity to *F.* PB1 SUP, indicating that butyrate is the main effector of *F.* PB1 activity.

Finally, we showed that the *F.* PB1 SUP also significantly reduced the dimensions of lesions in a model of inflammation-driven CRC (AOM and DSS), in which tumours preferentially develop in the colon, more closely mirroring the human pathology (Fig. 5h,i and Extended Data Fig. 6c).

Overall, these data show that due to their HDACi activity, the metabolic products of *F.* PB1—butyrate in particular—control NFATc3 activation, thereby blocking tumour cell proliferation in vivo in $Apc^{Min/+}$ mice independently of the microbiota. A similar anti-proliferative activity was also observed in an inflammation-driven CRC model.

The anti-proliferative activity of *F.* PB1 can be exerted by other SCFA-producing bacteria. We then evaluated whether the activity of *F.* PB1 is shared by other SCFA-producing bacteria. We selected *Lactococcus lactis*, because it secretes butyrate and some lactate in culture, similarly to *F.* PB1 (Extended Data Fig. 7a), and has been proposed to have anti-proliferative activities in vitro by an unknown mechanism[25]. We administered *L. lactis* following a schedule similar to that of *F.* PB1 but could not detect any anti-tumoural effect (Extended Data Fig. 7b,c). This is probably due to the inability of *L. lactis* to survive in or colonize the mouse intestine—as we could not detect *L. lactis*, even in WT mice—independently of the microbiota (Extended Data Fig. 7d). We thus analysed the anti-proliferative activity of the SUP from *L. lactis* in vivo in antibiotic-treated $Apc^{Min/+}$ mice. We found that the *L. lactis* SUP reduced the size of tumour lesions, although not as effectively as the *F.* PB1 SUP (Extended Data Fig. 7e,f). This difference cannot be due to a reduction in lactate production, as lactate did not impact on tumour cell proliferation in vitro (Extended Data Fig. 7g). The anti-proliferative activity of *F.* PB1 is therefore not unique to this bacterium and may be common to other bacteria that produce SCFAs, provided that they are able to colonize and/or survive in the intestine long enough to produce butyrate.

***H. biformis* is the equivalent of *F.* PB1 in humans**. We then assessed the relevance of these findings in human CRC. We interrogated a dataset of a shot-gun microbiome analysis carried out in patients with colorectal adenomas[26] and found that, similarly to the mouse, there was a reduction in the abundance of the family of Erysipelotrichaceae in patients with large adenomas compared with healthy individuals, but there was no change in the Shannon diversity index (Fig. 6a). In this family, an undefined genus ('*Erysipelotrichaceae noname*') and a species, *H. biformis*, were strongly under-represented in advanced colon adenomas (Fig. 6b). Interestingly, a high-quality phylogeny of the Erysipelotrichaceae family and the *F.* PB1 isolate showed that *H. biformis* is the second bacterium phylogenetically closest to *F.* PB1 among the bacteria that colonize the human gut (phylogenetic distance of 0.273; Fig. 6c).

Similarly to *F.* PB1, *H. biformis* released SCFAs (Fig. 6d) and the SUP of *H. biformis* inhibited human tumour cell proliferation (HT-29 and Caco-2; Extended Data Fig. 8a). This activity was mediated by the HDAC-inhibitory activity of the SUP, as shown by increased histone acetylation and reduced NFATc3 activation (Fig. 6e and Extended Data Fig. 8b). In vivo, *H. biformis* was unable to survive in or colonize the mouse intestine and we could not observe any anti-proliferative activity in $Apc^{Min/+}$ mice (Extended Data Fig. 8c–e). However, when we tested the *H. biformis* SUP in $Apc^{Min/+}$ mice, we observed a much higher effect on tumour multiplicity (Fig. 6f,g), suggesting that *H. biformis* may also have some effect on tumour initiation. This remains to be evaluated.

We confirmed our data on human specimens from CRC patients using a technology set up in our laboratory[27]. Tumour specimens from CRC patients were treated with the SCFA mix (acetate:propionate:butyrate, 2:1:1), *F.* PB1 SUP or *H. biformis* SUP. As shown in Fig. 6h and Extended Data Fig. 9a, the SUPs (*F.* PB1 and *H. biformis*) as well as the mix of SCFAs induced an increase in H3K27 acetylation and a reduction of NFATc3 protein levels. This correlated with reduced tumour cell proliferation, as shown by lower nuclear Ki67 immunostaining in the presence of either *F.* PB1 SUP (Extended Data Fig. 9b) or the SCFA combination (Extended Data Fig. 9c). These results suggest that *H. biformis* is the human counterpart of *F.* PB1.

Discussion

The mucus layer has been shown to undergo profound changes during CRC tumourigenesis, both in size and in composition due to epithelial cell dedifferentiation[28]. These changes may result in two concomitant and non-mutually exclusive events, which may be responsible for fostering intestinal tumourigenesis. On one hand, the increased penetrance or adherence of pro-tumourigenic bacteria may favour immune-cell recruitment and activation, drive tumour cell transformation or Th17 cell activation, thereby contributing to tumour development[7,29–35]. On the other hand, tumourigenesis may be due to the contraction of anti-tumourigenic bacteria that release anti-proliferative metabolites. We focused on the latter and identified a bacterial member of the murine gut microbiota, *F.* PB1, belonging to the Erysipelotrichaceae family, which is one of the most abundant taxa in the murine gut and is not expanded

Fig. 5 | The metabolic products of *F.* PB1, particularly butyrate, have an anti-proliferative activity in vivo that is independent of the microbiota. a,**b**, $Apc^{Min/+}$ mice were administered unfermented broth (Veh.) or *F.* PB1 SUP from week 8 to 10. Tumour multiplicity and tumour size were assessed at 10 weeks of age (**a**, left) and quantified (**a**, right). Data are from three independent experiments ($n = 13$ (Veh.) and 11 (SUP) mice). **c**–**e**, Eleven-week-old $Apc^{Min/+}$ mice were treated with antibiotics (ABX). After 2 d, mice were treated with Veh. or *F.* PB1 SUP three times (two administrations on the first day and one on the second day) in the presence of ABX. Mice were sacrificed 24 h after the last gavage and tumour multiplicity and tumour size were assessed (**c**). Data are from two independent experiments ($n = 6$ (Veh.) and 7 (SUP) mice). **f**,**g**, Eleven-week-old $Apc^{Min/+}$ mice were treated with ABX. After 2 d, mice were treated with vehicle, *F.* PB1 SUP or 1 mM butyrate (two administrations on the first day and one on the second day) in the presence of ABX. Mice were sacrificed 24 h after the last gavage (**f**, left). Data are from two independent experiments ($n = 7$ (Veh.) and 8 (SUP and butyrate) mice). **a**,**c**,**f**, Tumour multiplicity in the small intestine normalized to vehicle-treated $Apc^{Min/+}$ mice (right). **b**,**d**,**g**, Area (right) and maximum diameter (left) of ileal dysplastic lesions normalized to the total number lesions per mouse. **e**, Representative images of ileal dysplastic lesions stained with anti-NFATc3 antibody (×200 magnification) or with anti-histone H3 acetyl K27 antibody (×100 magnification). Scale bars, 100 µm (NFATc3) and 200 µm (H3K27ac). Quantitative colour deconvolution analysis of histone H3 acetylation in dysplastic lesions of $Apc^{Min/+}$ mice treated with or without SUP ($n = 6$ (Veh.) and 4 (SUP) biologically independent samples; right). **h**,**i**, C57BL/6 WT mice were treated with AOM. After 3 d, mice underwent two cycles of 7 d DSS and 14 d recovery. During the second recovery, mice received vehicle ($n = 5$ mice) or *F.* PB1 SUP ($n = 6$ mice) three times per week for two weeks (**h**, left). Data from one experiment are depicted. **h**, Tumour multiplicity in the colon normalized to vehicle-treated $Apc^{Min/+}$ mice (right). **i**, Area (right) and maximum diameter (left) of colon adenomas normalized to the total number of lesions per mouse. Two (**c**–**i**) or three (**a**,**b**) independent experiments were performed with consistent results. **a**–**i**, Data are represented as the mean ± s.e.m. **b**,**d**,**g**,**i**, The box plots show the interquartile range, the horizontal lines show the median values and the whiskers indicate the minimum-to-maximum range. *P* values were evaluated using a two-tailed unpaired Mann–Whitney *U*-test (**a**–**e**,**h**), Kruskal–Wallis test with Dunn's post-hoc test (**f**,**g**) or two-tailed unpaired Student's *t*-test (**i**); n.s., not significant.

during tumourigenesis, presumably due to the different mucus composition. This may explain why its contraction affects tumour development so drastically.

Tumourigenesis in human CRC and Apc$^{Min/+}$ mice is dependent on the calcineurin-mediated activation of the NFATc3 transcription factor, which drives tumour cell proliferation[23]. NFATc3 is also involved in driving the expression of MUC5ac[36], which may explain why hCRC and Apc$^{Min/+}$ mice ectopically express MUC5ac. Calcineurin can be induced to degradation by the HDACi panobinostat[24]. Here, we show that the SUPs from *F.* PB1 and its human counterpart, *H. biformis*, act as an HDACi affecting calcineurin and NFATc3 activation, and this results in the inhibition of tumour cell growth independently of the microbiota (Extended Data Fig. 10). In some cases, we also observed an effect of *F.* PB1 or *H. biformis* SUP on tumour multiplicity. This could be due to a technical issue as a result of the inability to also detect small tumours but we cannot exclude an effect on tumour initiation.

We found a reduction of lactate in the faeces of mice treated with *F.* PB1. This was unexpected, as *F.* PB1 was found to produce large quantities of lactate in vitro, but we cannot anticipate whether it was also produced in vivo. In addition, as lactate is known to be produced and used by tumour cells[37,38], the reduction of lactate after *F.* PB1 administration could be due to either reduced tumour cell proliferation or increased use of lactate by the tumour cells.

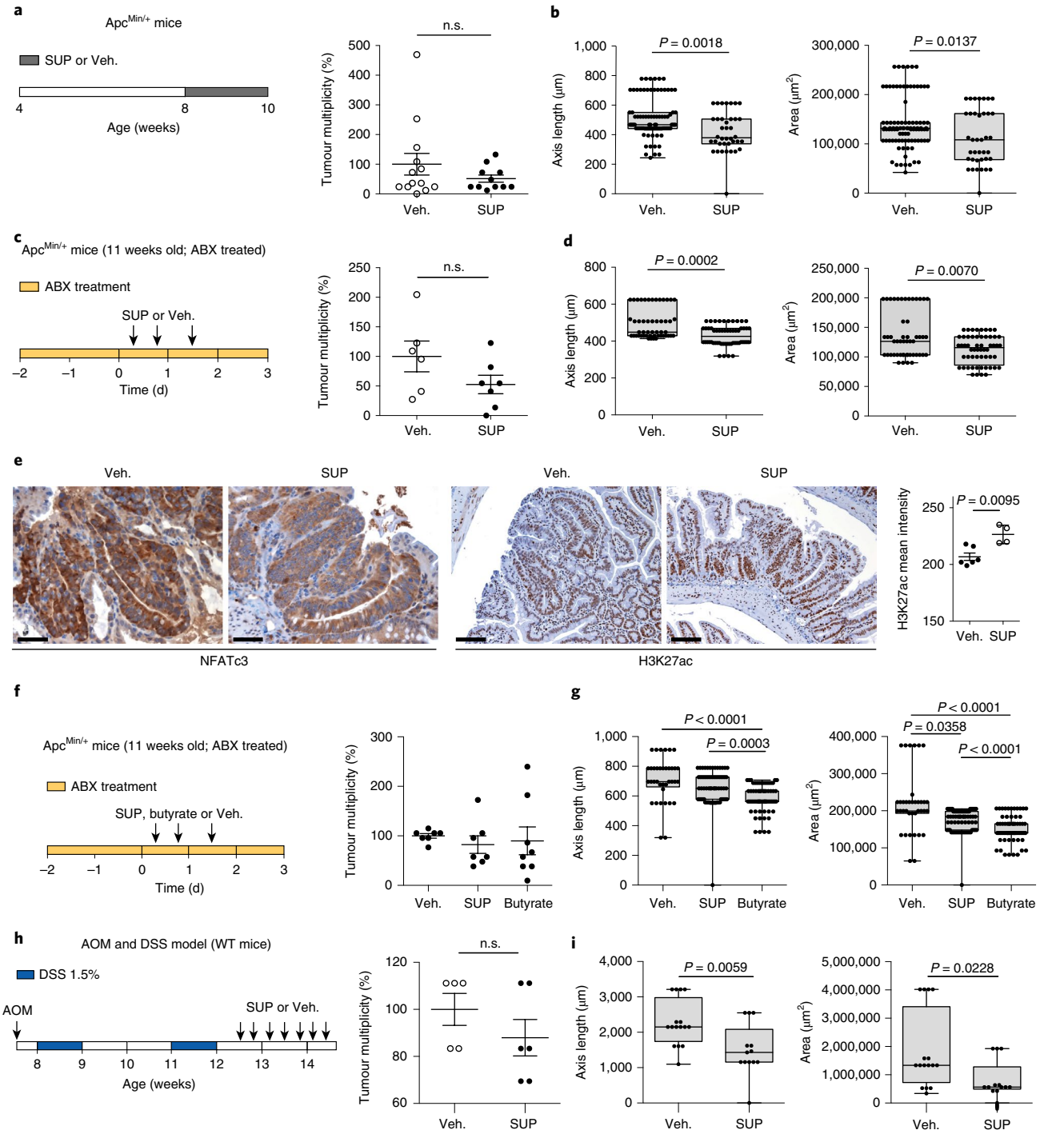

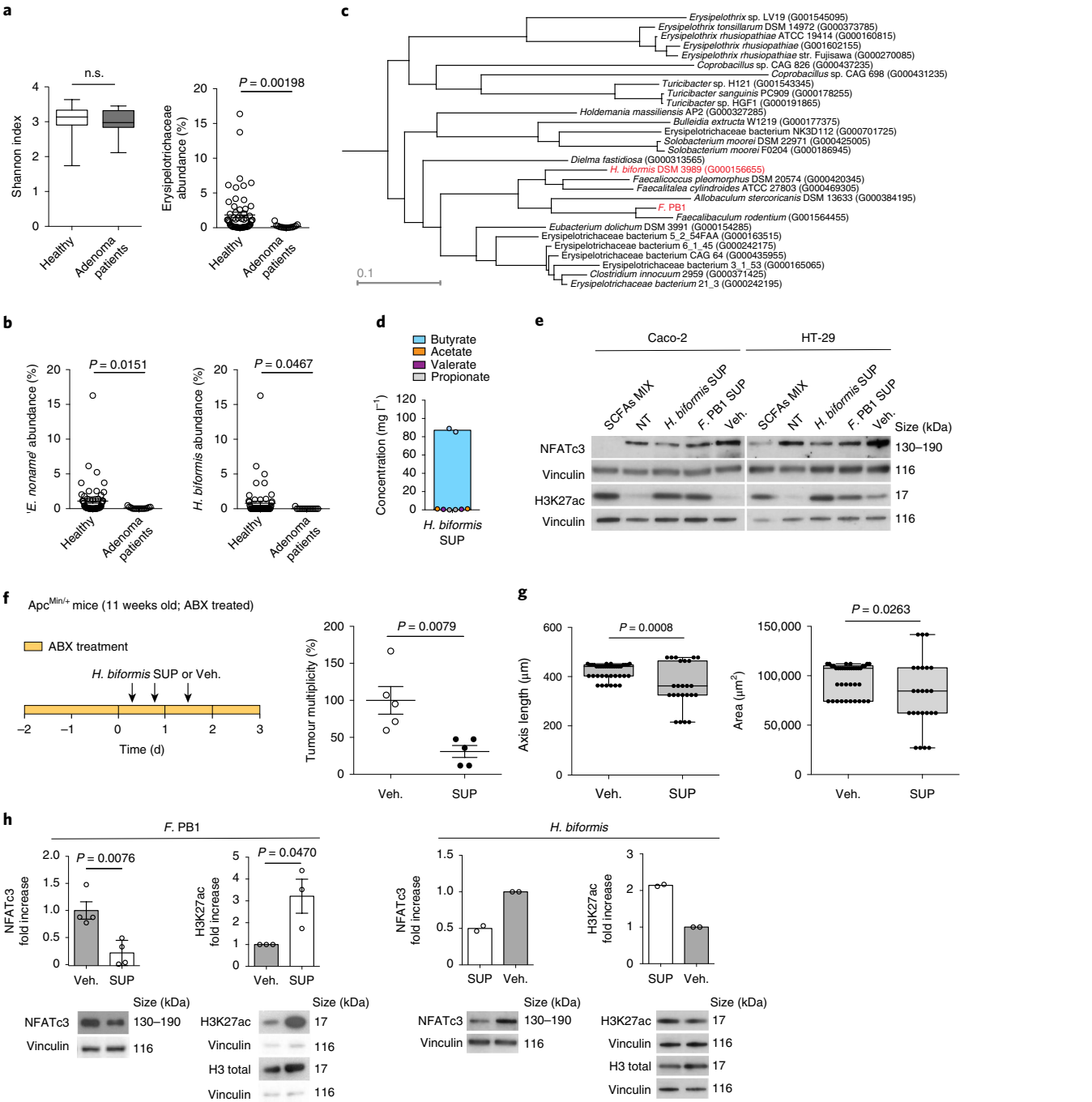

Fig. 6 | *H. biformis* is the equivalent of *F.* PB1 in humans. a, Shannon diversity index (left) and abundance of the family Erysipelotrichaceae (right) in faecal DNA from healthy donors ($n=61$) and patients with large adenoma ($n=15$). **b**, Abundance of the undefined genus '*E. noname*' and the species *H. biformis*. A two-tailed Wilcoxon rank-sum test comparing the relative abundances of large adenoma ($n=15$) and control ($n=61$) samples was applied at each taxonomic level. *P* values obtained at the family and genus taxonomic levels were corrected for multiple hypothesis testing using the Benjamin–Hochberg procedure. **c**, High-quality phylogeny of the Erysipelotrichaceae family and the *F.* PB1 isolate. **d**, Levels of SCFAs in the broth fermented by *H. biformis* (*H. biformis* SUP), determined using UPLC–HR–MS. Data are from $n=2$ biologically independent experiments. **e**, Representative western blot from two or three independent experiments performed with consistent results showing the effect of SCFAs MIX, *F.* PB1 SUP and *H. biformis* SUP on H3K27 acetylation and NFATc3 expression in human CRC cell lines. Cells that were not treated (NT) or treated with non-fermented medium (Veh.) served as controls. Vinculin was used as a loading control. The densitometric analysis is reported in Extended Data Fig. 8b. **f**,**g**, Eleven-week-old $Apc^{Min/+}$ mice were treated with antibiotics (ABX). After 2 d, mice were treated with vehicle or *H. biformis* SUP for three times (two administrations on the first day and one on the second day) in the presence of ABX. Mice were sacrificed 24 h after the last gavage ($n=5$ mice per group). **f**, Tumour multiplicity in the small intestine normalized to vehicle-treated $Apc^{Min/+}$ mice. **g**, Area (right) and maximum diameter (left) of ileal dysplastic lesions normalized to the total number of lesions per mouse. **h**, Representative western blot from two or three independent experiments performed with consistent results showing the effect of *F.* PB1 SUP and *H. biformis* SUP on H3K27 acetylation and NFATc3 expression in ex vivo-treated hCRC samples (bottom). The bar plots (top) show the densitometric quantification of NFATc3 (normalized to vinculin) and H3K27 acetylation (normalized to total H3; $n=2$ (*H. biformis* SUP) and 3 (*F.* PB1 SUP) biologically independent experiments). **a**,**b**,**d**,**f**–**h**, Data are represented as the mean ± s.e.m. *P* values were evaluated using a two-tailed unpaired Mann–Whitney *U*-test (**a**,**f** and **g**, right) and two-tailed unpaired Student's *t*-test (**g**, left panel and **h**). **a**,**g**, The box plots show the interquartile range, the horizontal lines show the median values and the whiskers indicate the minimum-to-maximum range.

Alternatively, lactate could be used by other bacterial species for their own growth[39].

The involvement of SCFAs in the observed anti-proliferative activity is demonstrated by the following observations: evaporation to deplete SCFAs led to a strong reduction in the activity of the SUP and the SUP from another butyrate-producing bacterium (*L. lactis*) or butyrate itself can mimic the effect of *F.* PB1 at a concentration similar to that found in the SUP. This suggests that the antitumour activity of *F.* PB1 is not unique and could be shared with other SCFA-producing bacteria as long as they have the ability to colonize or survive in the gut and produce butyrate locally.

Why does butyrate only inhibit proliferation of tumour cells and not normal epithelial cells? In CRC, tumour cells undergo increased glycolysis rather than mitochondrial oxidative metabolism due to the Warburg effect[21]. Thus, cancer cells do not use butyrate for their growth, the butyrate concentration increases and can act as HDACi[22]. Consistent with this, dietary fibres, which promote the growth of butyrate-producing bacteria, affect tumourigenesis in $Apc^{Min/+}$ mice[12] and $Apc^{Min/+}$ mice with a deleted *niacr1* are more susceptible to tumour development via a mechanism that depends on the microbiota[19].

Consistent with data in the literature[40,41], we have shown that *H. biformis* is able to produce SCFAs and its spent medium can inhibit tumour cell proliferation. We do not know whether *H. biformis*, similarly to mouse *F.* PB1, is the major bacterium responsible for the antitumour properties in humans or whether other SCFA-producing bacteria are also contracted in humans and may contribute to failure of tumour-growth control. Future studies should aim at addressing this point and assessing whether this species may have a therapeutic potential. As *H. biformis* is reduced in the faeces of patients with large adenomas, it may also be used as a potential biomarker for detecting tumours in their early phase.

Methods

Bacterial strains. *F.* PB1 was isolated in the Kenya Honda laboratory (RIKEN IMS) from the faecal pellets of 12-week-old WT C57BL/6 littermates of our $Apc^{Min/+}$ colony as described previously[42]. Briefly, the faeces were suspended in tryptic soy broth, serially diluted and plated on Eggerth–Gagnon (EG) agar plates. Forty-eight colonies were picked and sequenced using pan-bacterial primers targeting the 16S rRNA gene. Similarity to *F. rodentium* was checked against both databases and the sequence retrieved from our metagenomic analysis, resulting in 99.7 and 98% homology, respectively. The *F.* PB1 strain was deposited to the German collection of microorganisms DSMZ (type strain no. DSM32803). *H. biformis* was purchased from the DSMZ (type strain no. 3989). Both bacteria were cultured in an anaerobic chamber (gas atmosphere N_2:CO_2:H_2 of 80:15:5) in pre-reduced EG broth under anaerobic conditions for 48 h. The bacterial strain *Lactococcus lactis* subsp. *lactis* was purchased from DSMZ (type strain no. 20481) and cultured in pre-reduced MRS broth at 30 °C in static conditions. Bacterial SUP was derived from overnight cultures of the strains in the conditions described above. The medium fermented by the bacteria (SUP) was filtered in 0.25 µm filters and immediately frozen.

Cell lines. The mouse (CT26) and human (HT-29 and Caco-2) CRC cell lines were purchased from the American Type Culture Collection. The CMT-93 mouse rectum carcinoma cell line was a gift from D. Artis (Cornell University). The MC-38 mouse carcinoma cell line was a gift from C. Krieg (Zurich University). The APC cell line was derived from $Apc^{Min/+}$ small-intestinal adenomas by mechanical disruption. No further authentication method was performed on the purchased cell lines. The loss of heterozygosity (loss of the WT allele and presence of the Min allele) in the APC cell line was checked using a TaqMan assay. CT26 cells were cultured in RPMI 1640 medium supplemented with 10% FBS and 2 mM L-glutamine. CMT-93 and MC-38 cells were cultured in DMEM medium supplemented with 10% FBS and 2 mM L-glutamine. APC cells were cultured in complete DMEM medium supplemented with insulin-transferrin-selenium-ethanolamine (ITS-X, Gibco) and human EGF (10 pg µl^{-1}). HT-29 cells were cultured in DMEM medium supplemented with 10% FBS and 2 mM L-glutamine. Caco-2 cells were cultured in MEM medium with Earle's Salt supplemented with 20% FBS, 2 mM L-glutamine, 1 mM sodium pyruvate and 0.1 mM non-essential amino acids. All of the cell lines were tested to exclude mycoplasma contamination.

To evaluate the effect of SCFA (either alone or in combination) and the bacterial SUP, cells were seeded and stimulated after an overnight incubation. The cells were stimulated with sodium acetate (S5636, Sigma-Aldrich), sodium propionate (P5436, Sigma-Aldrich), sodium butyrate (ARK2161, Sigma-Aldrich) or a mix of the three. APC, CT26, MC-38, HT-29 and Caco-2 cells were stimulated with 50 mM sodium acetate, 10 mM sodium propionate, 2 mM sodium butyrate or a mix of 50 mM sodium acetate, 10 mM propionate and 2 mM butyrate. CMT-93 cells were stimulated with 10 mM sodium acetate, 2.5 mM sodium propionate, 1 mM sodium butyrate or a mix of 10 mM sodium acetate, 2.5 mM propionate and 1 mM butyrate. The cells were also stimulated with different concentrations (0.8, 4, 20 mM) of sodium L-lactate (cat. no. 71718, Sigma-Aldrich). Finally, cells were stimulated with the bacterial broth diluted 40% (v/v) in cell culture medium (EG broth) fermented by *F.* PB1 or *H. biformis* (SUP) or relative control non-fermented broth (vehicle). In addition, CT26 cells were treated with the fermented broth (also called spent medium) that had been evaporated to remove the SCFAs. The spent medium was evaporated to dryness at 50 °C under reduced pressure (5 mbar). The residue was taken up with water, filtered and diluted 40% (v/v) in cell culture medium.

Following 48 h of stimulation, the proliferation of the cells was evaluated using a CyQUANT cell proliferation assay (Molecular Probes). Each condition was tested in six wells of a 96-multiwell plate and 12 reads per well were recorded.

Mice. This study employed both male and female mice from the C57BL6/J, C57BL6/J-ApcMin/J and germ-free ICR strains as model organisms. Six-week-old C57BL6/J mice were purchased from Harlan Laboratories. C57BL6/J-Apc^{Min}/J (referred to as $Apc^{Min/+}$; ref. [43]) mice were maintained as an inbred strain in our animal facility. For experiments where $Apc^{Min/+}$ mice were employed, WT littermates born from the same mothers of experimental mice were used as controls. All of the mice were maintained in micro-isolator cages in a specific-pathogen-free animal facility. Germ-free ICR male mice were maintained in the isolators at RIKEN IMS. Experiments were performed in accordance with the guidelines established in the Principles of Laboratory Animal Care (directive 86/609/EEC) and approved by the Italian Ministry of Health. On the basis of our experience with animal models and according to animal-welfare policy (directive 86/609/EEC), which strongly suggests the use of a limited number of animals, we estimated that two experiments with $n=5$ mice per group would allow us to reach statistical significance. Animals were randomly allocated to each treatment group. The different treatment groups were processed identically and animals in the different treatment groups were exposed to the same environment. The investigators were not blinded during experimental mice allocation and outcome assessment. For the macroscopic analysis of the tumour lesions, we first calculated the average of tumour numbers in the vehicle group; the number of tumours of an individual mouse is referred as a percentage of this average.

Bacterial profiling of intestinal microbiota. DNA from faecal pellets and mucus scraped from the small intestine and colon was extracted using a GNOME DNA isolation kit (MP) following a published protocol[44]. The V5–V6 hypervariable regions of the bacterial 16S rRNA genes were amplified and processed with a modified version of the Nextera protocol[45]. The metagenomic libraries obtained were sequenced using a MiSeq Illumina platform with a 2×250 paired-end approach. Metagenomic amplicons were analysed by applying the BioMaS pipeline[46]. First, the paired-end reads were merged into consensus sequences using PEAR[47] and subsequently dereplicated applying Usearch[48], maintaining the information about the total number of reads supporting each consensus sequence. Second, the paired-end reads that remained non-overlapping were only considered for further analysis if both read ends were ≥50 bp long after the low-quality region trimming (Phred quality cut-off=25). Third, both the merged sequences and the unmerged reads were matched against the Ribosomal Database Project database (release 11.2)[49] using Bowtie2 (ref. [50]). The mapping data were filtered according to two parameters: identity percentage and query coverage (≥70%). In particular, sequences that yielded an identity percentage ≥97% were classified to species level and those with identity ≥90% and <97% were classified at a higher taxonomic rank. Finally, all mapped reads fulfilling the settled filters were taxonomically annotated using the Tango tool[51]. The assigned genera were filtered—only those for which at least five reads per samples were considered present. The read counts were normalized using an approach similar to the RPKM (reads per kilo-base per million): normalized count = assigned reads ÷ (total assigned reads at the rank level ÷ 1,000,000). The statistical differences between the faecal microbiota at the genus and species level of WT and $Apc^{Min/+}$ mice were calculated using the DESeq2 R package[52]. Taxa specifically associated with one of the analysed conditions were identified using the linear discriminant analysis effect size (LEfSe)[53].

The *F.* PB1 abundance was validated using a qPCR assay with specific primers and normalized to pan-bacterial primers targeting the 16S rRNA gene (UNI 16S)[54]. The bacterial primer sequences are listed in Supplementary Table 1.

Normalized read counts for differentially represented species in WT and $Apc^{Min/+}$ mice were log-transformed and plotted as a heat map using the vegan[55] and the ggplot2[56] R packages.

Histological evaluation. Formalin-fixed and paraffin-embedded swiss rolls of colon and small intestine were sectioned to thicknesses of 3–4 mm and the sections were stained with haematoxylin and eosin. For histopathological examination and scoring, the haematoxylin and eosin slides were evaluated by an expert pathologist. The extent of inflammatory changes was defined according to the score proposed

by Cooper and colleagues[57]. The histological scoring system to evaluate the colitis grade is described in Supplementary Table 2. The number of ulcers and dysplastic/adenomatous lesions was also reported for each sample. The proliferative lesions are classified according to mouse pathology consensus recommendations[58]. The tissue area of dysplastic and adenomatous lesions was measured on haematoxylin and eosin-stained slides using digital microscopy. Briefly, the slides were digitalized by an Aperio ScanScope CS Slide Scanner (Aperio Technologies) at ×40 magnification. The dysplastic and adenomatous lesions were identified and selected using Aperio ImageScope (Leica Biosystems Imaging). The value of every selected dysplastic/adenomatous area is expressed in μm^2 and its major axis in µm.

Fluorescence in situ hybridization. Tissues were fixed with Carnoy's solution and paraffin embedded, and were then sectioned to a thickness of 5 µm. The probes used were designed to specifically target different regions of the *F.* BPI 16S rRNA. All of the probes were manufactured by Sigma and labelled with cyanine 3 (Cy3; 5′-(Cy3)GCCAACCAACTAATGCACCG and 5′-(CY3) CCGGGAATACGCTCTGGAAA). The probes were used at 5 ng μl^{-1} in pre-warmed hybridization buffer (0.9 M NaCl, 20 mM Tris pH 7.4 and 0.01% SDS). The slides were incubated at 55 °C in a humid chamber for 90 min, washed twice in pre-warmed washing buffer (0.9 M NaCl and 20 mM Tris pH 7.4) at 55 °C, mounted and counterstained with 4,6-diamidino-2-phenylindole (DAPI; contained in the VECTASHIELD mounting medium). Confocal images were acquired using a Leica DMi8 confocal microscope with a HCX PL APO ×40 (NA 1.25) oil-immersion objective.

Immunofluorescence. To maintain the mucus structure, the murine intestines were fixed in Carnoy fixative (60% ethanol, 30% chloroform and 10% acetic acid, glacial), manually processed, paraffin embedded and stored at room temperature until microtome sectioning. Microsections (6 µm thick) were cut using a microtome (Leica), mounted on Ultra plus poly-L-lysine-coated glass slides (Menzel–Glaser) and left at 37 °C overnight. The tissue sections were deparaffinized in histolemon and hydrated through a graded ethanol series (100%, 95% and 70%, followed by H_2O). Antigen unmasking was performed in Tris–EDTA pH 9 (10 mM Tris–HCl, 1 mM EDTA and 0.05% Tween 20) for 50 min at 95 °C. The sections were incubated overnight with the anti-muc1 rabbit polyclonal primary antibody (1:100; clone aa474–630; LS-C343984, LifeSpan Bioscience) at +4 °C. After two wash steps in 0.1 M Tris pH 7.4, the slides were incubated with the donkey anti-rabbit-Cy3 secondary antibody (1:300; cat. no. 711165153, Jackson Immuno Research) for 2 h at room temperature. After washing twice in 0.1 M Tris pH 7.4 for 10 min, the slides were counterstained and mounted with VECTASHIELD mounting medium with DAPI (Vector Laboratories). Confocal images were acquired with a Leica DMi8 confocal microscope and a HCX PL APO ×40 (NA 1.25) oil-immersion objective. All images were adjusted and assembled in Fiji software.

RNA extraction, RT–PCR and qPCR. Intestinal chunks from WT mice, normal ileal chunks and pooled small intestinal polyps from $Apc^{Min/+}$ mice were sampled from 8- and 16-week-old mice. The intestinal tissue was homogenized in 500 µl TRIzol (Invitrogen). RNA was extracted by adding 100 µl chloroform and precipitating the aqueous phase with one volume of 100% ethanol, followed by purification of the RNA with a Quick-RNA miniprep kit (Zymo Research). The RNA was retro-transcribed using a ImProm-II reverse transcriptase kit (Promega). The qPCR assay was performed using the Fast SYBR green master mix (Life Technologies). The primers used are listed in Supplementary Table 1. The expression levels were normalized to the expression of the 60S ribosomal protein gene *Rpl32*.

Human metagenomics. For the analysis of the Zeller et al.[26] CRC dataset, raw sequences were downloaded from the sequence read archive and used as input into MetaPhlAn2 (ref. [59]). Individual sample profiles were merged and the final table was filtered to include only members of the Erysipelotrichaceae family and the samples collected in France. The generated taxonomic profiles are available through the curatedMetagenomicData resource[60]. At each taxonomic level, we applied a Wilcoxon rank-sum test comparing the relative abundances of the large adenoma ($n = 15$) and control ($n = 61$) samples. *P* values obtained at each taxonomic level were corrected for multiple hypothesis testing using the Benjamin–Hochberg procedure. A high-quality phylogeny of the Erysipelotrichaceae family based on the 400 PhyloPhlAn[61] markers considering 47 complete reference genomes deposited in the NCBI (the accession nos are reported in parentheses in the node labels) and the *F.* PB1 isolate was performed.

Samples from human patients. Colonic human specimens were obtained from patients diagnosed with colon cancer and undergoing surgery at European Institute of Oncology (IEO). The inclusion criteria were: newly diagnosed CRC patients (stage I to III) aged between 35 and 70 years old, a performance status of 0–1 based on the Eastern Cooperative Oncology Group and signed informed consent according to the International Council for Harmonisation of Technical Requirements for Pharmaceuticals for Human Use (ICH)-Good Clinical Practice (GCP). Exclusion criteria were: a personal history of malabsorption syndrome or any chronic inflammatory bowel disease, patients with hereditary syndrome (such as familial adenomatous polyposis and hereditary non-polyposis colorectal cancer) and use of antibiotics in the previous four weeks. All patients gave informed written consent and were enrolled in the institutional protocol approved by IEO's ethical committee. Human biological samples were sourced ethically and their research use was in accordance with the terms of the informed consent provided. Case selection was therefore independent and blinded to baseline characteristics, treatments received, clinical outcome and molecular characterization to reduce any potential self-selection bias.

Administration of *F.* PB1 to germ-free mice, and *F.* PB1, *H. biformis* and *L. lactis* to $Apc^{Min/+}$ mice. In experiments of gnotobiotic colonization, five germ-free ICR male mice were administered 250 µl *F.* PB1 culture (optical density $(OD)_{600} \cong 0.6$; corresponding to about 5×10^7 c.f.u. ml^{-1}) orally and the abundance of small-intestinal and colonic cells was addressed after 4 weeks. To evaluate the effect of exogenous *F.* PB1 administration, WT and $Apc^{Min/+}$ mice were administered frozen bacterial stocks equivalent to 250 µl of culture at the logarithmic growth phase orally 3× a week, according to different schedules (see Figs. 2d,e and 3c). The mice were sacrificed at the age of 8, 10 or 12 weeks and the tumour multiplicity in the small intestine and colon was assessed. Neutrophil and inflammatory monocyte abundances in circulating blood and regulatory T, Th1 and Th17 cell abundances in the small intestinal and colonic lamina propria were assessed. The bleeding score was assigned as follows: 0, negative to Hemoccult (Beckman Coulter); 1, positive to Hemoccult and 2, gross bleeding. To evaluate the effect of exogenous *H. biformis* and *L. lactis* administration, $Apc^{Min/+}$ mice were administered frozen bacterial stocks orally 3× a week from the age of 8–10 weeks. In the monocolonization experiments, WT and $Apc^{Min/+}$ mice were treated with or without antibiotic cocktail (1 g l^{-1} ampicillin, 1 g l^{-1} neomycin and 0.5 g l^{-1} vancomycin in their drinking water and 2 mg metronidazole administered by oral gavage every 2 d) for 7 d and challenged with vehicle, *F.* PB1 or *L.lactis* for 3 d in a row. The mice were sacrificed after 48 h and the bacterial abundance was validated in the faeces, and ileal and colon mucus using a qPCR assay with specific primers (Supplementary Table 1).

Spent medium administration to $Apc^{Min/+}$ mice or C57BL6/J WT mice treated with AOM and DSS. Eight-week-old C57BL6/J mice were treated with AOM (10 mg kg^{-1} body weight) by intraperitoneal injection. After 3 d, they received DSS 1.5% (w/v) in their drinking water for 7 d. The mice were allowed to recover for 14 d. This schedule was repeated for two cycles. During the second recovery (from week 12 to 14), the mice were treated with EG broth fermented by *F.* PB1 (*F.* PB1 SUP) or relative control non-fermented broth (vehicle) by oral gavage (200 µl per mouse) 3× per week for two weeks and the tumour lesions were analysed.

Culture broths fermented with *F.* PB1, *H. biformis* or *L.lactis* (*F.* PB1 SUP, *H. biformis* SUP or *L.lactis* SUP) or not (vehicle) were administered by oral gavage 3× per week for two weeks to eight-week-old $Apc^{Min/+}$ mice.

Vehicle (EG for *F.* PB1 or *H.biformis*; MRS broth for *L.lactis*), SUP and butyrate (1 mM) were also administered by oral gavage (200 µl per mouse) 3× in a row (twice on day 1) in combination with the antibiotic cocktail (1 g l^{-1} ampicillin, 1 g l^{-1} neomycin and 0.5 g l^{-1} vancomycin in their drinking water and 2 mg metronidazole administered by oral gavage every 2 d) to 11-week-old $Apc^{Min/+}$ mice pretreated with the antibiotic cocktail for 2 d. In these experiments, the mice were sacrificed 24 h after the last gavage.

Quantification of faecal and spent-medium SCFAs. The SCFAs in the faecal and SUP (*F.* PB1, *H. biformis* and *L. lactis*) samples were quantified as previously described[62], with a few modifications. In detail, 100 mg faeces or 200 µl SUP was resuspended in 2 ml of 0.001% HCOOH and vortexed for 1 min. The suspension was centrifuged at 1,000*g* for 2 min at 4 °C and the supernatant was recovered. The residue was extracted again as described above. The supernatants were combined and the volume was adjusted to 5 ml with a solution of 0.001% HCOOH in water. All extracts were stored at −20 °C. Before UPLC–HR-MS analysis, the samples were diluted 1:100 in 0.001% HCOOH and centrifuged at 3,000*g* for 1 min. The UPLC–HR-MS analysis was carried out on an Acquity UPLC separation module (Waters) coupled with an Exactive Orbitrap MS with an HESI-II probe for electrospray ionization (Thermo Scientific). The ion source and interface conditions were as follows: spray voltage, −3.0 kV; sheath-gas flow rate, 35 ml min^{-1}; auxiliary-gas flow rate, 10 ml min^{-1}; temperature, 120 °C; and capillary temperature, 320 °C. A 1.8-mm HSS T3 column (150 × 2.1 mm; Waters) was used for separation at a flow rate of 0.2 ml min^{-1}. The eluents were 0.001% HCOOH in MilliQ-treated water (solvent A) and CH_3OH:CH_3CN (1:1 (v/v); solvent B). A 5 µl aliquot of the sample was separated by UPLC using the following elution gradient: 0% B for 4 min, 0–15% B over 6 min, 15–20% B over 5 min, 20% B for 13 min, followed by a return to the initial conditions in 1 min. The column and samples were maintained at 30 and 15 °C, respectively. The UPLC eluate was analysed using full-scan mass spectrometry in the range 50–130 *m/z*. The resolution was set at 50 K, the AGC target was 1×10^6 and the maximum ion-injection time was 100 ms. The ion with a *m/z* of 91.0038, corresponding to the HCOOH dimer $(2M–H)^-$, was used as the lock mass. The mass tolerance was 2 ppm. The mass spectrometry data were processed using the Xcalibur software (Thermo Scientific). Analytical grade

SCFAs were used as standards (Sigma-Aldrich). Five-point external calibration curves were adopted to quantify the pyruvic, lactic, succinic, acetic, propionic, butyric, isobutyric, valeric and isovaleric acids in the faecal samples. The SCFA concentrations were expressed in millimoles per 100 g of wet faeces.

Flow cytometry. Peripheral blood was sampled in heparin and the red blood cells were lysed. The samples were stained with anti-CD45.2, -CD3, -Ly6C, -Ly6G and -CD11b antibodies. Neutrophils were defined as $Ly6G^{+}CD11b^{+}$ and inflammatory monocytes as $Ly6C^{high}CD11b^{+}$ in the $CD45^{+}CD3^{-}$ population. Small intestinal and colonic lamina propria lymphocytes were isolated by incubating intestinal chunks in PBS, 5% FCS, 1.5 mM EDTA and 1 mM dithiothreitol at 37 °C for 15 min to remove the epithelial cells. The lamina propria cells were mechanically isolated in RPMI medium containing 5% FCS using a GentleMACS dissociator. The cells were permeabilized using a FoxP3 intracellular staining kit (eBioscience) and stained with anti-CD45.2, -CD3, -CD4, -CD25, -FoxP3 and -Helios antibodies. For Th1 and Th17 detection, the lamina propria cells were incubated for 4 h with phorbol myristate acetate (50 ng ml^{-1}; Sigma-Aldrich), ionomycin (500 ng ml^{-1}; Sigma-Aldrich) and GolgiStop (BD Biosciences). The cells were then stained with anti-CD45.2, -CD3, -CD4, -IL17 PE and -IFNγ antibodies. For mononuclear phagocytes identification, the lamina propria cells were stained with anti-CD45.2, -CD11, -F4/80, -CD11c, -Ly6G and -Ly6C antibodies. Dead cells were excluded with the Fixable Viability Stain510 (BD Biosciences). Samples were acquired using FACSCantoII and Fortessa (BD Biosciences) and analysed with FlowJo (Treestar). See Supplementary Table 3 for detailed information.

Western blotting. For western blot analysis, cells and tissue samples were lysed using RIPA buffer (50 mM Tris–HCl pH 8, 150 mM NaCl, 1 mM EDTA, 1% Triton X-100, 1% sodium deoxycholate and 0,1% SDS) supplemented with protease inhibitors (cOmplete Mini, EDTA-free; Roche), and tyrosine protein-, acid- and alkaline-phosphatase inhibitors (Phosphatase inhibitor cocktail 2, Sigma-Aldrich) 48 h after stimulation, and the lysates were sonicated. The proteins in freshly prepared cell lysates were measured using a Bradford assay (Bio-Rad) and equal amounts of the proteins were run on a SDS–PAGE gel, followed by western blotting. After 30 min at room temperature in blocking solution—5% milk or 5% BSA in Tris-buffered saline and Tween 20 (TBST; 10 mM Tris pH 7.5, 150 mM NaCl and 0.1% (v/v) Tween 20)—the membranes were probed with primary antibodies in 5% milk (or 5% BSA) in TBST overnight at 4 °C, washed in TBST and incubated for 1 h at room temperature with secondary antibodies: goat anti-rabbit–horseradish peroxidase (HRP; 1:10,000; cat. no. 170-6515, Bio-Rad), goat anti-mouse–HRP (1:10,000; cat. no. 170-6516, Bio-Rad) or rabbit anti-goat–HRP (1:2,000; P0449, DAKO). The following primary antibodies were used: anti-PP2B-A (1:1,000, clone H-209; sc-9070, Santa Cruz Biotechnology), anti-NFATc3 (1:1,000, polyclonal (M-75) or monoclonal (F-1); sc-8321 and sc-8405, respectively, Santa Cruz Biotechnology), anti-histone H3 acetyl K27 (1:1,000; ab4729, Abcam), anti-histone H3 (1:1,000; ab1791, Abcam), anti-actin (1:1000; A4700, Sigma), anti-muc1 (1:200, clone F-19; sc-6826, Santa Cruz Biotechnology); anti-muc13 (1:1,000; ab124654, Abcam); anti-muc20 (1:1,000; PA5-50238, Thermofisher). Visualization was carried out using chemiluminescence (Clarity Western ECL substrate, Bio-Rad or ECL, Amersham). Densitometric quantification was performed using Fiji software.

Immunohistochemistry. Formalin-fixed paraffin-embedded sections were deparaffinized and rehydrated through an ethanol series. Antigen unmasking was performed in 1 mM EDTA pH 8 for 50 min at 95 °C. Endogenous peroxidases were quenched with 3% H_2O_2 (SZBF1960V, Sigma). The human sample slides were incubated with anti-Ki67 antibody (1:200; ab15580, Abcam) or anti-NFATc3 polyclonal (1:200, sc-8321, Santa Cruz Biotechnology), whereas the mouse sample slides were incubated with anti-NFATc3 monoclonal (1:200; sc-8405, Santa Cruz Biotechnology; unmasking in EDTA pH 8 for 40 min at 98 °C) for 2 h at room temperature. For acetylation visualization, antigen unmasking was performed in 10 mM sodium citrate and 0.05% Tween 20, pH 6.0 for 20 min at 95 °C. After peroxidase quenching, the slides were incubated for 1 h with anti-histone H3 acetyl K27 (1:500 for human and 1:800 for mouse tissues; ab4729, Abcam). After washing, the slides were incubated with Envision system HRP rabbit (K4003, DAKO) and developed with 3,3′-diaminobenzidine (DAB) solution (K3468, DAKO). The slides were counterstained with haematoxylin and mounted. The DAB^{+} signal was quantified using Fiji software with the ImmunoRatio plugin[63].

Ex vivo stimulation of human colonic mucosa. The human colonic specimens were obtained from patients diagnosed with colon cancer and undergoing surgery at the IEO, following informed consent, according to the ICH-GCP. The protocol was approved by the IEO's ethical committee. Ex vivo organ cultures were performed on colonic tumour mucosa specimens according to the protocol of Tsilingiri and colleagues[27]. Briefly, tumour specimens were cut into pieces of about 0.5 cm^2 and placed on sterile metal grids in a centre-well organ-culture plate containing 1 ml medium (DMEM supplemented with 2 mM glutamine, 15% FBS–Na, 1% ITS-X and 200 ng ml^{-1} EGF). The tissues were incubated overnight in a 100% O_2 atmosphere at a pressure of 1 atm inside an airtight container at 37 °C. Colonic tissues were either fixed in 4% paraformaldehyde and processed for histological and immunohistochemistry analyses or snap frozen for protein extraction.

To evaluate the effect of SCFAs on human colon tumours and controls, the medium was supplemented with 200 mM sodium acetate (S5636, Sigma-Aldrich), 100 mM sodium propionate (P5436, Sigma-Aldrich) and 100 mM sodium butyrate (ARK2161, Sigma-Aldrich) at a ratio similar to that found in the faecal content of *F.* PB1-treated mice (acetate:propionate:butyrate, 2:1:1). To evaluate the effect of *F.* PB1- or *H. biformis*-produced SCFAs, fermented EG broth (SUP) was added to the medium at a concentration of 40%; non-fermented EG broth (Veh.) was used as a control. Tumour tissues were either processed for immunohistochemistry or lysed, and the H3 acetylation and NFATc3 levels were analysed.

Statistical analysis. Data were analysed for normal distribution before any statistical analyses. Data analyses were carried out using GraphPad Prism version 6.01b. Values are presented as the mean ± s.e.m. or mean ± s.d.; individual values are presented as scatter plots with column bar graphs or as box plots showing the interquartile range, median and minimum-to-maximum whiskers. Outliers were detected using Grubbs' test and excluded from the analysis. Statistical significance between two groups was determined using two-tailed unpaired Student's *t*-test, multiple *t*-tests corrected for multiple comparisons using the Holm–Sidak method, the Mann–Whitney *U*-test or Wilcoxon's rank-sum test, whereas the comparison of multiple groups was carried out using the Kruskal–Wallis test followed by Dunn's test and one- or two-way ANOVA, followed by Bonferroni's or Tukey's post-hoc test. The Benjamini–Hochberg procedure was used to adjust *P* values for multiple testing. The data displayed normal variance. A probability value of $^{*}P < 0.05$ was considered significant. All statistics and reproducibility information are reported in the figure legends. Sample size was chosen by taking the means of the target values between the experimental group and the control group, the standard error and the statistical analysis used into consideration. For the animal studies, sample size was defined on the basis of past experience with the models. The minimum number of animals necessary to achieve the scientific objectives was used for ethical reasons. Animals were allocated randomly to each treatment group. Different treatment groups were processed identically and animals in different treatment groups were exposed to the same environment. In the immunohistochemistry and immunofluorescence analyses, the investigators were unaware of the experimental groups.

Reporting Summary. Further information on research design is available in the Nature Research Reporting Summary linked to this article.

Data availability

Source Data for the figures and Extended Data figures are provided in the online version of the paper. Raw sequencing data and metadata associated to samples are available online at the NCBI under the accession number PRJNA564752.

Received: 11 December 2018; Accepted: 26 November 2019;
Published online: 27 January 2020

References

1. Sears, C. L. & Garrett, W. S. Microbes, microbiota, and colon cancer. *Cell Host Microbe* **15**, 317–328 (2014).
2. Kostic, A. D. et al. Genomic analysis identifies association of *Fusobacterium* with colorectal carcinoma. *Genome Res.* **22**, 292–298 (2012).
3. Mima, K. et al. *Fusobacterium nucleatum* in colorectal carcinoma tissue according to tumor location. *Clin. Transl. Gastroenterol.* **7**, e200 (2016).
4. Yu, T. et al. *Fusobacterium nucleatum* promotes chemoresistance to colorectal cancer by modulating autophagy. *Cell* **170**, 548–563 (2017).
5. Kinzler, K. W. & Vogelstein, B. Lessons from hereditary colorectal cancer. *Cell* **87**, 159–170 (1996).
6. Li, Y. et al. Gut microbiota accelerate tumor growth via c-jun and STAT3 phosphorylation in $APC^{Min/+}$ mice. *Carcinogenesis* **33**, 1231–1238 (2012).
7. Kostic, A. D. et al. *Fusobacterium nucleatum* potentiates intestinal tumorigenesis and modulates the tumor-immune microenvironment. *Cell Host Microbe* **14**, 207–215 (2013).
8. Wu, S. et al. A human colonic commensal promotes colon tumorigenesis via activation of T helper type 17 T cell responses. *Nat. Med.* **15**, 1016–1022 (2009).
9. Arthur, J. C. et al. Intestinal inflammation targets cancer-inducing activity of the microbiota. *Science* **338**, 120–123 (2012).
10. Zhan, Y. et al. Gut microbiota protects against gastrointestinal tumorigenesis caused by epithelial injury. *Cancer Res.* **73**, 7199–7210 (2013).
11. Wong, S. H. et al. Gavage of fecal samples from patients with colorectal cancer promotes intestinal carcinogenesis in germ-free and conventional mice. *Gastroenterology* **153**, 1621–1633 (2017).
12. Donohoe, D. R. et al. A gnotobiotic mouse model demonstrates that dietary fiber protects against colorectal tumorigenesis in a microbiota- and butyrate-dependent manner. *Cancer Discov.* **4**, 1387–1397 (2014).
13. Chang, D. H. et al. *Faecalibaculum rodentium* gen. nov., sp. nov., isolated from the faeces of a laboratory mouse. *Antonie Van Leeuwenhoek* **108**, 1309–1318 (2015).

14. Johansson, M. E. et al. The inner of the two Muc2 mucin-dependent mucus layers in colon is devoid of bacteria. *Proc. Natl Acad. Sci. USA* **105**, 15064–15069 (2008).
15. Xiao, X. et al. Role of MUC20 overexpression as a predictor of recurrence and poor outcome in colorectal cancer. *J. Transl. Med.* **11**, 151 (2013).
16. Betge, J. et al. MUC1, MUC2, MUC5AC, and MUC6 in colorectal cancer: expression profiles and clinical significance. *Virchows Arch.* **469**, 255–265 (2016).
17. Guglietta, S. et al. Coagulation induced by C3aR-dependent NETosis drives protumorigenic neutrophils during small intestinal tumorigenesis. *Nat. Commun.* **7**, 11037 (2016).
18. Sakamoto, M., Tanaka, Y., Benno, Y. & Ohkuma, M. *Butyricimonas faecihominis* sp. nov. and *Butyricimonas paravirosa* sp. nov., isolated from human faeces, and emended description of the genus *Butyricimonas*. *Int. J. Syst. Evol. Microbiol.* **64**, 2992–2997 (2014).
19. Singh, N. et al. Activation of gpr109a, receptor for niacin and the commensal metabolite butyrate, suppresses colonic inflammation and carcinogenesis. *Immunity* **40**, 128–139 (2014).
20. Boffa, L. C., Vidali, G., Mann, R. S. & Allfrey, V. G. Suppression of histone deacetylation in vivo and in vitro by sodium butyrate. *J. Biol. Chem.* **253**, 3364–3366 (1978).
21. Vander Heiden, M. G., Cantley, L. C. & Thompson, C. B. Understanding the Warburg effect: the metabolic requirements of cell proliferation. *Science* **324**, 1029–1033 (2009).
22. Donohoe, D. R. et al. The Warburg effect dictates the mechanism of butyrate-mediated histone acetylation and cell proliferation. *Mol. Cell* **48**, 612–626 (2012).
23. Peuker, K. et al. Epithelial calcineurin controls microbiota-dependent intestinal tumor development. *Nat. Med.* **22**, 506–515 (2016).
24. Imai, Y. et al. Histone deacetylase inhibitor panobinostat induces calcineurin degradation in multiple myeloma. *JCI Insight* **1**, e85061 (2016).
25. Han, K. J., Lee, N. K., Park, H. & Paik, H. D. Anticancer and anti-inflammatory activity of probiotic *Lactococcus lactis* NK34. *J. Microbiol. Biotechnol.* **25**, 1697–1701 (2015).
26. Zeller, G. et al. Potential of fecal microbiota for early-stage detection of colorectal cancer. *Mol. Syst. Biol.* **10**, 766 (2014).
27. Tsilingiri, K., Sonzogni, A., Caprioli, F. & Rescigno, M. A novel method for the culture and polarized stimulation of human intestinal mucosa explants. *J. Vis. Exp.* **75**, e4368 (2013).
28. Kesari, M. V. et al. Immunohistochemical study of MUC1, MUC2 and MUC5AC in colorectal carcinoma and review of literature. *Indian J. Gastroenterol.* **34**, 63–67 (2015).
29. Yan, X., Liu, L., Li, H., Qin, H. & Sun, Z. Clinical significance of *Fusobacterium nucleatum*, epithelial–mesenchymal transition, and cancer stem cell markers in stage III/IV colorectal cancer patients. *Onco Targets Ther.* **10**, 5031–5046 (2017).
30. Bullman, S. et al. Analysis of *Fusobacterium* persistence and antibiotic response in colorectal cancer. *Science* **358**, 1443–1448 (2017).
31. Mendes, R. T. et al. Endothelial cell response to *Fusobacterium nucleatum*. *Infect. Immun.* **84**, 2141–2148 (2016).
32. Gur, C. et al. Binding of the Fap2 protein of *Fusobacterium nucleatum* to human inhibitory receptor TIGIT protects tumors from immune cell attack. *Immunity* **42**, 344–355 (2015).
33. Chen, Y. et al. Invasive *Fusobacterium nucleatum* activates beta-catenin signaling in colorectal cancer via a TLR4/P-PAK1 cascade. *Oncotarget* **8**, 31802–31814 (2017).
34. Chung, L. et al. *Bacteroides fragilis* toxin coordinates a pro-carcinogenic inflammatory cascade via targeting of colonic epithelial cells. *Cell Host Microbe* **23**, 203–214 (2018).
35. Dejea, C. M. et al. Patients with familial adenomatous polyposis harbor colonic biofilms containing tumorigenic bacteria. *Science* **359**, 592–597 (2018).
36. Yan, F. et al. Interleukin-13-induced MUC5AC expression is regulated by a PI3K–NFAT3 pathway in mouse tracheal epithelial cells. *Biochem. Biophys. Res. Commun.* **446**, 49–53 (2014).
37. San-Millan, I. & Brooks, G. A. Reexamining cancer metabolism: lactate production for carcinogenesis could be the purpose and explanation of the Warburg effect. *Carcinogenesis* **38**, 119–133 (2017).
38. Faubert, B. et al. Lactate metabolism in human lung tumors. *Cell* **171**, 358–371 (2017).
39. Duncan, S. H., Louis, P. & Flint, H. J. Lactate-utilizing bacteria, isolated from human feces, that produce butyrate as a major fermentation product. *Appl. Environ. Microbiol.* **70**, 5810–5817 (2004).
40. Zhernakova, A. et al. Population-based metagenomics analysis reveals markers for gut microbiome composition and diversity. *Science* **352**, 565–569 (2016).
41. De Maesschalck, C. et al. *Faecalicoccus acidiformans* gen. nov., sp. nov., isolated from the chicken caecum, and reclassification of *Streptococcus pleomorphus* (Barnes et al. 1977), *Eubacterium biforme* (Eggerth 1935) and *Eubacterium cylindroides* (Cato et al. 1974) as *Faecalicoccus pleomorphus* comb. nov., *Holdemanella biformis* gen. nov., comb. nov. and *Faecalitalea cylindroides* gen. nov., comb. nov., respectively, within the family Erysipelotrichaceae. *Int. J. Syst. Evol. Microbiol.* **64**, 3877–3884 (2014).
42. Atarashi, K. et al. Treg induction by a rationally selected mixture of clostridia strains from the human microbiota. *Nature* **500**, 232–236 (2013).
43. Moser, A. R., Pitot, H. C. & Dove, W. F. A dominant mutation that predisposes to multiple intestinal neoplasia in the mouse. *Science* **247**, 322–324 (1990).
44. Furet, J. P. et al. Comparative assessment of human and farm animal faecal microbiota using real-time quantitative PCR. *FEMS Microbiol. Ecol.* **68**, 351–362 (2009).
45. Manzari, C. et al. Draft genome sequence of *Sphingobium* sp. strain ba1, resistant to kanamycin and nickel ions. *FEMS Microbiol. Lett.* **361**, 8–9 (2014).
46. Fosso, B. et al. BioMaS: a modular pipeline for bioinformatic analysis of metagenomic amplicons. *BMC Bioinform.* **16**, 203 (2015).
47. Zhang, J, Kobert, K, Flouri, T. & Stamatakis, A. PEAR: a fast and accurate Illumina paired-end read merger. *Bioinformatics* **30**, 614–620 (2014).
48. Edgar, R. C. Search and clustering orders of magnitude faster than BLAST. *Bioinformatics* **26**, 2460–2461 (2010).
49. Cole, J. R. et al. The ribosomal database project: improved alignments and new tools for rRNA analysis. *Nucleic Acids Res.* **37**, D141–D145 (2009).
50. Langmead, B. & Salzberg, S. L. Fast gapped-read alignment with Bowtie 2. *Nat. Methods* **9**, 357–359 (2012).
51. Alonso-Alemany, D. et al. Further steps in TANGO: improved taxonomic assignment in metagenomics. *Bioinformatics* **30**, 17–23 (2014).
52. Love, M. I., Huber, W. & Anders, S. Moderated estimation of fold change and dispersion for RNA-seq data with DESeq2. *Genome Biol.* **15**, 550 (2014).
53. Segata, N. et al. Metagenomic biomarker discovery and explanation. *Genome Biol.* **12**, R60 (2011).
54. Salzman, N. H. et al. Enteric salmonella infection inhibits Paneth cell antimicrobial peptide expression. *Infect. Immun.* **71**, 1109–1115 (2003).
55. Oksanen, J. et al. Vegan: community ecology package. R package vegan version 2.2-1 (2015); https://cran.r-project.org/web/packages/vegan/index.html
56. Wickham, H. *ggplot2: Elegant Graphics for Data Analysis* (Springer, 2009).
57. Cooper, H. S., Murthy, S. N., Shah, R. S. & Sedergran, D. J. Clinicopathologic study of dextran sulfate sodium experimental murine colitis. *Lab. Invest.* **69**, 238–249 (1993).
58. Boivin, G. P. et al. Pathology of mouse models of intestinal cancer: consensus report and recommendations. *Gastroenterology* **124**, 762–777 (2003).
59. Truong, D. T. et al. MetaPhlAn2 for enhanced metagenomic taxonomic profiling. *Nat. Methods* **12**, 902–903 (2015).
60. Pasolli, E. et al. Accessible, curated metagenomic data through ExperimentHub. *Nat. Methods* **14**, 1023–1024 (2017).
61. Segata, N., Bornigen, D., Morgan, X. C. & Huttenhower, C. PhyloPhlAn is a new method for improved phylogenetic and taxonomic placement of microbes. *Nat. Commun.* **4**, 2304 (2013).
62. Gargari, G. et al. Consumption of a *Bifidobacterium bifidum* strain for 4 weeks modulates dominant intestinal bacterial taxa and fecal butyrate in healthy adults. *Appl. Environ. Microbiol.* **82**, 5850–5859 (2016).
63. Tuominen, V. J., Ruotoistenmaki, S., Viitanen, A., Jumppanen, M. & Isola, J. ImmunoRatio: a publicly available web application for quantitative image analysis of estrogen receptor (ER), progesterone receptor (PR), and Ki-67. *Breast Cancer Res.* **12**, R56 (2010).

Acknowledgements

We thank M. Bugatti and S. Licini (supported by Fondazione Beretta, Brescia, Italy) for their technical support in the histological analyses; A. Thomas and E. Pasolli for performing the bioinformatics analyses; C. Faccani for technical support for the in vitro experiments; and E. Mileti, C. Burrello and M. R. Giuffré for their technical support for the in vivo experiments. This work has been supported by grants from the Italian Association for Cancer Research (grant no. AIRC IG 17628) and the European Research council (grant no. 615735, HOMEOGUT ERC) to M.R. E.Z., I.S. and A.B. were/are recipients of a FIRC fellowship. T.S. is a recipient of a fellowship from Fondazione Veronesi. G.F. is a recipient of a grant from the Italian Ministry of Health (grant no. GR-2013-02359806).

Author contributions

E.Z. and C.P. ideated, performed and analysed all of the experiments. T.S. and F.S. helped with the execution of experiments. A.B., I.S. and S.Guglietta helped with the execution of the mouse experiments. B.F., M.M. and G.Pesole performed the 16S rRNA metagenomic analysis. L.M. and W.V. designed and carried out the histological analyses. G.N. performed the ex vivo stimulation of human colonic mucosa experiments. A.B.

performed the confocal analyses. J.T. executed the metabolomic analyses. B.O. assisted in the execution of the in vitro experiments. K.A. and K.H. isolated *F.* PB1 and carried out the germ-free experiments. S.A. and S.Guglielmetti set up *F.* PB1 growth and supernatant production. S.C. set up *H. biformis* and *L. lactis* growth and supernatant production. G.F. performed the FACS analyses. F.A. and N.S. performed the phylogenetic analysis and human CRC dataset interrogation. G.Penna contributed with ideas and interpretation of results. M.R. ideated the study, coordinated the work and wrote the manuscript.

Competing interests

The authors declare no competing interests.

Additional information

Extended data is available for this paper at https://doi.org/10.1038/s41564-019-0649-5.

Supplementary information is available for this paper at https://doi.org/10.1038/s41564-019-0649-5.

Correspondence and requests for materials should be addressed to M.R.

Reprints and permissions information is available at www.nature.com/reprints.

Publisher's note Springer Nature remains neutral with regard to jurisdictional claims in published maps and institutional affiliations.

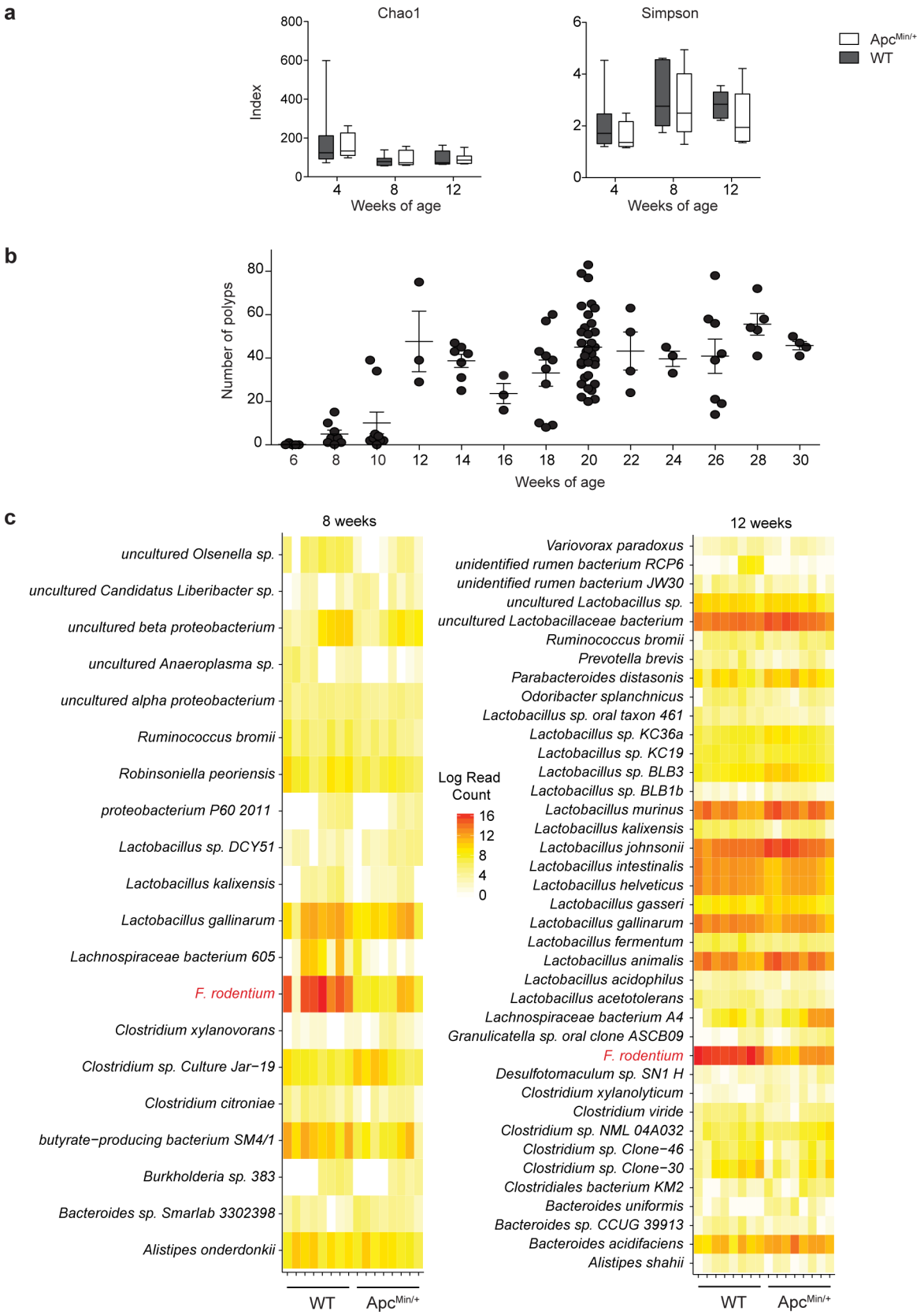

Extended Data Fig. 1 | Faecal microbiota diversity upon tumour progression in $Apc^{Min/+}$ mice. a, Chao1 and Simpson indexes of the faecal microbiota of WT and $Apc^{Min/+}$ mice; n = 8 mice/group. Box plots show the interquartile range, median value and whiskers min to max. Data from two independent experiments. **b**, Tumour multiplicity in the small intestine of $Apc^{Min/+}$ mice assessed at different time points; weeks 6, 28 n = 5; weeks 8, 26 n = 8; weeks 10 n = 9; weeks 12, 16, 24 n = 3; weeks 14 n = 7; weeks 18 n = 10; weeks 20 n = 33; weeks 22, 30 n = 4 mice/group. **c**, Normalized read counts for differentially represented species in WT and $Apc^{Min/+}$ mice shown as heatmaps. The counts were log transformed and used to define the colour gradient of the heatmap; n = 8 mice/group. Data from two independent experiments. **a**-**c**, Data are represented as means ± s.e.m.

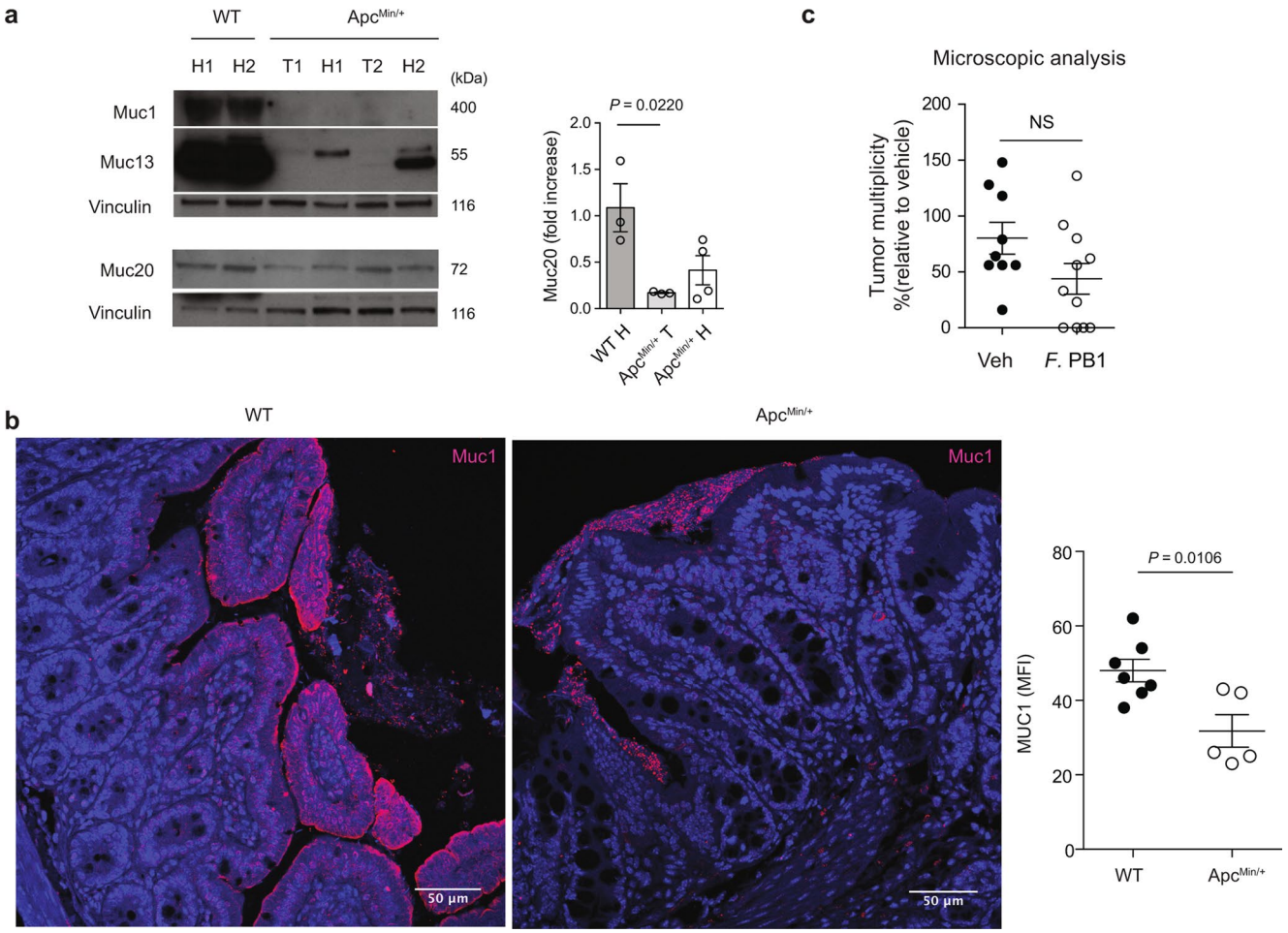

Extended Data Fig. 2 | Mucin production is altered in the ileum of Apc$^{Min/+}$ mice. a, Representative Western blots of two independent experiments with consistent results showing the abundance of Muc1, Muc13 and Muc20 in ileal extracts from WT (healthy tissues, H) and healthy (H) and tumour (T) tissues of Apc$^{Min/+}$ mice analysed at 11 weeks of age; Right: densitometric quantification (WT n = 3; Apc$^{Min/+}$ n = 4 biologically independent samples). **b**, Representative confocal images of WT and Apc$^{Min/+}$ mice ileum intestinal tissues stained with Muc1 (red) and DAPI (blue); scale bars, 50 µm. Mean fluorescence intensity of MUC1 was measured to quantify the expression of the protein in the intestinal of Apc$^{Min/+}$ and WT mice (WT n = 7, Apc$^{Min/+}$ n = 5 biologically independent samples). **c**, Apc$^{Min/+}$ mice were treated with vehicle (n = 10 mice/group) or *F.* PB1 (n = 11 mice/group) from week 8 to 10. Number of microscopic lesions, shown as % relative to vehicle, was evaluated on H&E slides by an expert pathologist. **a**-**c**, Data from two independent experiments and represented as means ± s.e.m. *P* values were determined by one-way ANOVA using Tukey post-test (**a**), two-tailed unpaired Mann Whitney U test (**b**), or two-tailed unpaired Student's *t*-test (**c**).

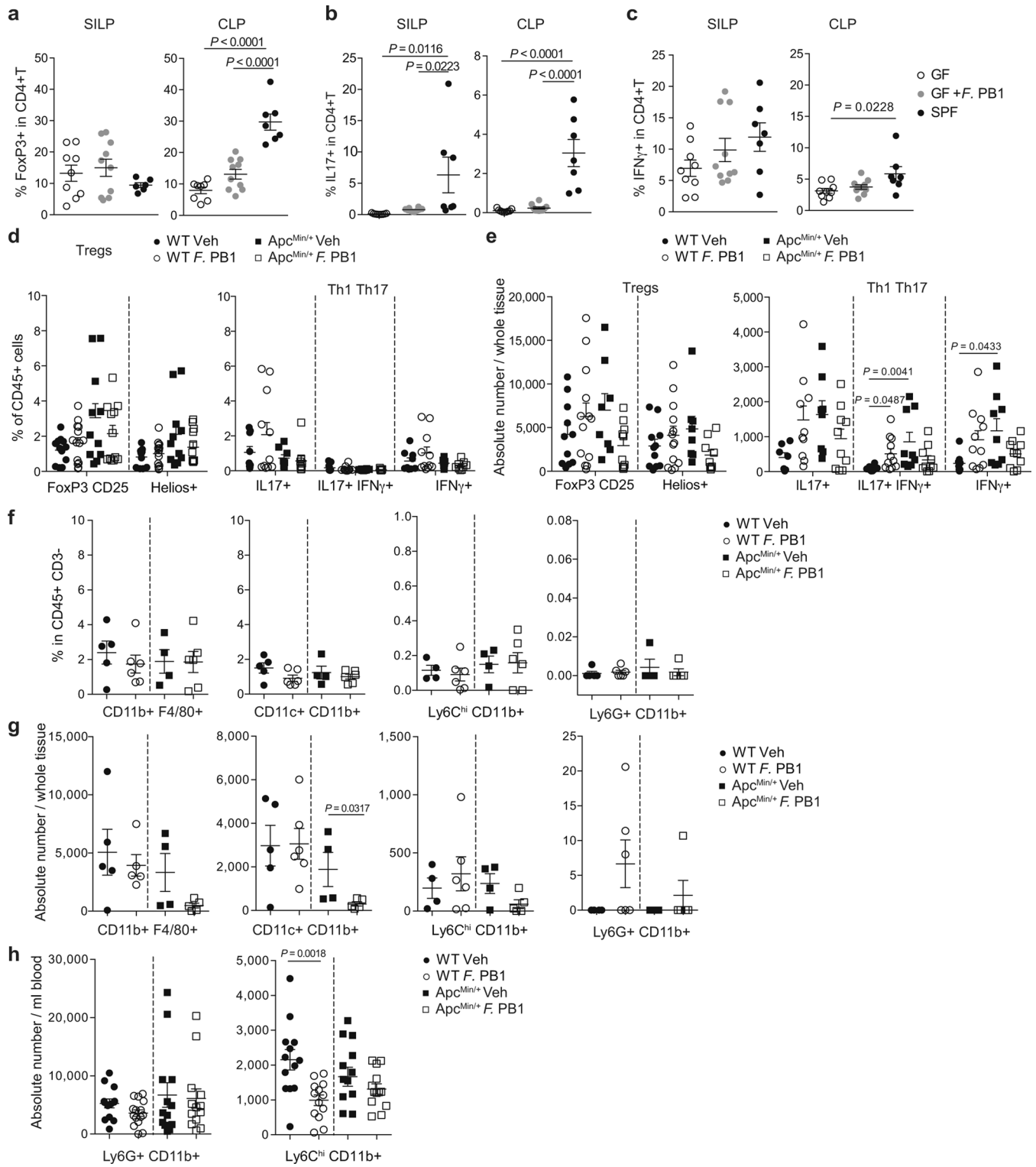

Extended Data Fig. 3 | See next page for caption.

Extended Data Fig. 3 | *F.* PB1 does not have a major impact on immune cells. a-**c**, Flow cytometry analyses of the small intestinal and colonic lamina propria of germ-free ICR mice monocolonized with *F.* PB1 (GF + *F.* PB1 n = 10 mice/group) for the presence of T reg (**a**), Th17 (**b**) and Th1 (**c**) cells. Germ-free (GF, n = 9 mice/group) and SPF (n = 7 mice/group) mice were used as controls. **d**-**g** WT and $Apc^{Min/+}$ mice treated with vehicle (Veh) or *F.* PB1 from week 8 to 12. **d**,**e**, Flow cytometric analysis of T reg, Th1 and Th17 cell populations in the small intestinal lamina propria. FoxP3+CD25+ are gated on the live CD45+ CD3+ CD4+ cells; Helios+ is gated on the FoxP3+ CD25+ cells (WT Veh, $Apc^{Min/+}$ *F.* PB1 n = 12; WT *F.* PB1 n = 14; $Apc^{Min/+}$ Veh n = 11 mice/group). IL17+, IFNγ+ and IL17+ IFNγ+ cells are gated on the live CD45+ CD3+ CD4+ cells (WT Veh, $Apc^{Min/+}$ Veh n = 9; WT *F.* PB1 n = 11; $Apc^{Min/+}$ *F.* PB1 n = 10 mice/group). Data shown as % of CD45+ cells (**d**) or as absolute number / whole tissue (**e**). **f**,**g**, Flow cytometric analysis of mononuclear phagocytes (CD11b+F4/80+ macrophages, CD11c+CD11b+ dendritic cells and $Ly6C^{hi}$CD11b+ inflammatory monocytes) and neutrophils (Ly6G+CD11b+) in the small intestinal lamina propria (WT Veh n = 5; WT *F.* PB1, $Apc^{Min/+}$ *F.* PB1 n = 6; $Apc^{Min/+}$ Veh n = 4). Data shown as percentages relative to the CD45+ CD3- population (**f**) or as absolute number / whole tissue (**g**). **h**, Flow cytometric analysis of peripheral blood cells. Data shown as absolute number / ml blood (WT Veh, $Apc^{Min/+}$ *F.* PB1 n = 13; WT *F.* PB1 n = 15; $Apc^{Min/+}$ Veh n = 12 mice/group) *P* values were determined by one-way ANOVA with Bonferroni post-test (**a**-**d**), Kruskal-Wallis with Dunn post test (**e**), two-tailed unpaired Mann-Whitney U test (**f**,**g**,**h** Ly6G+CD11b+) or two-tailed unpaired Student's *t*-test (**h**, $Ly6C^{hi}$CD11b+). **a**-**h**, Data are represented as means ± s.e.m.

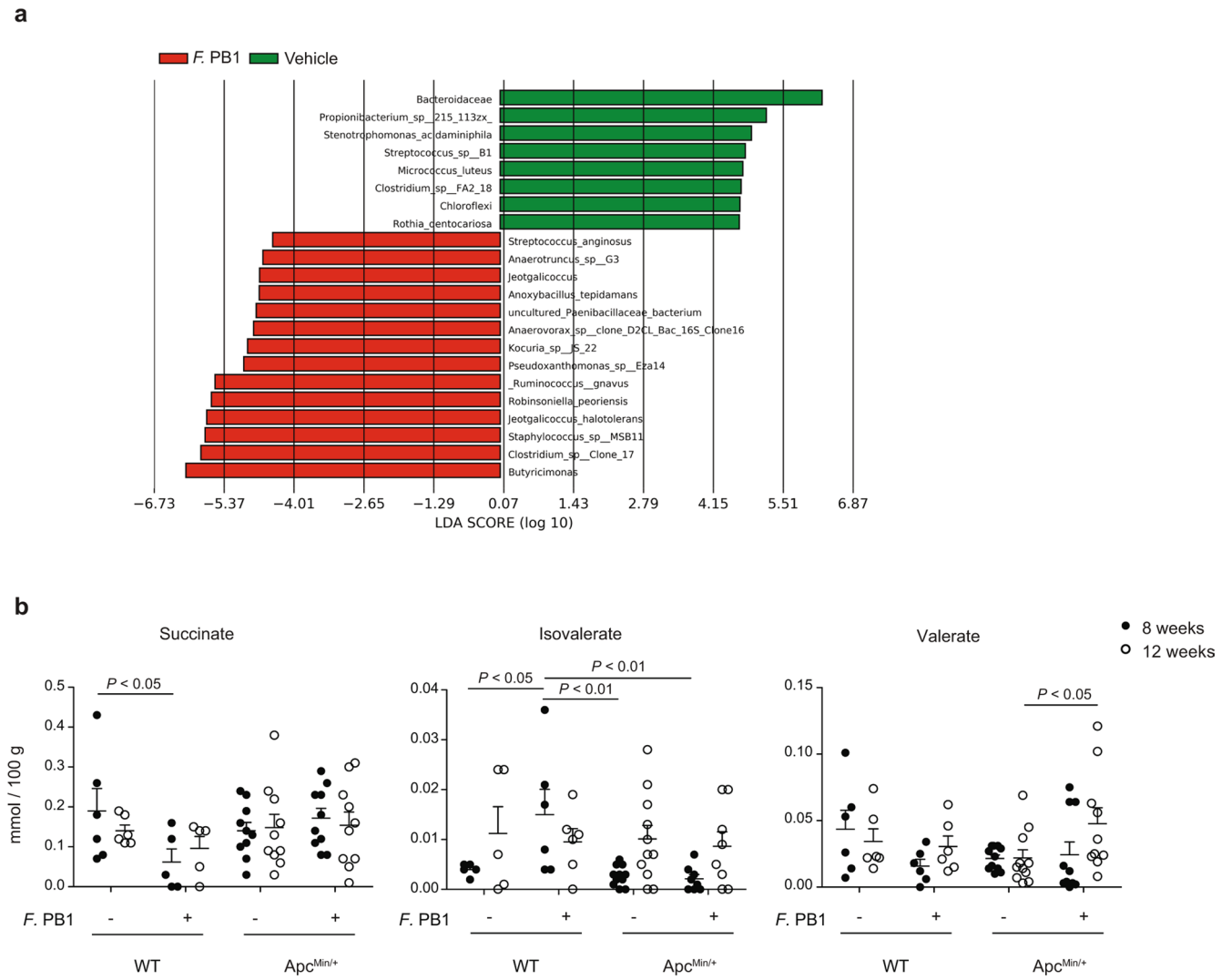

Extended Data Fig. 4 | *F.* PB1 administration alters microbiota and its metabolic profile. a, LEfSe comparison results between the microbiota of Vehicle and *F.* PB1 treated mice at 12 weeks with the highest linear discriminant analysis LDA score (log10 ≥ 2.0); Veh, n = 8; *F.* PB1 n = 14 mice/group. **b**, Faecal concentrations of succinate, isovalerate and valerate in WT and $Apc^{Min/+}$ mice treated with vehicle (Veh) or *F.* PB1 as detected by UPLC–HR–MS; WT Veh, WT *F.* PB1 n = 6; $Apc^{Min/+}$ Veh n = 11; $Apc^{Min/+}$ *F.* PB1 n = 10 mice/group. Data from two independent experiments and represented as means ± s.e.m. *P* values were determined by two-way ANOVA with Bonferroni post-test.

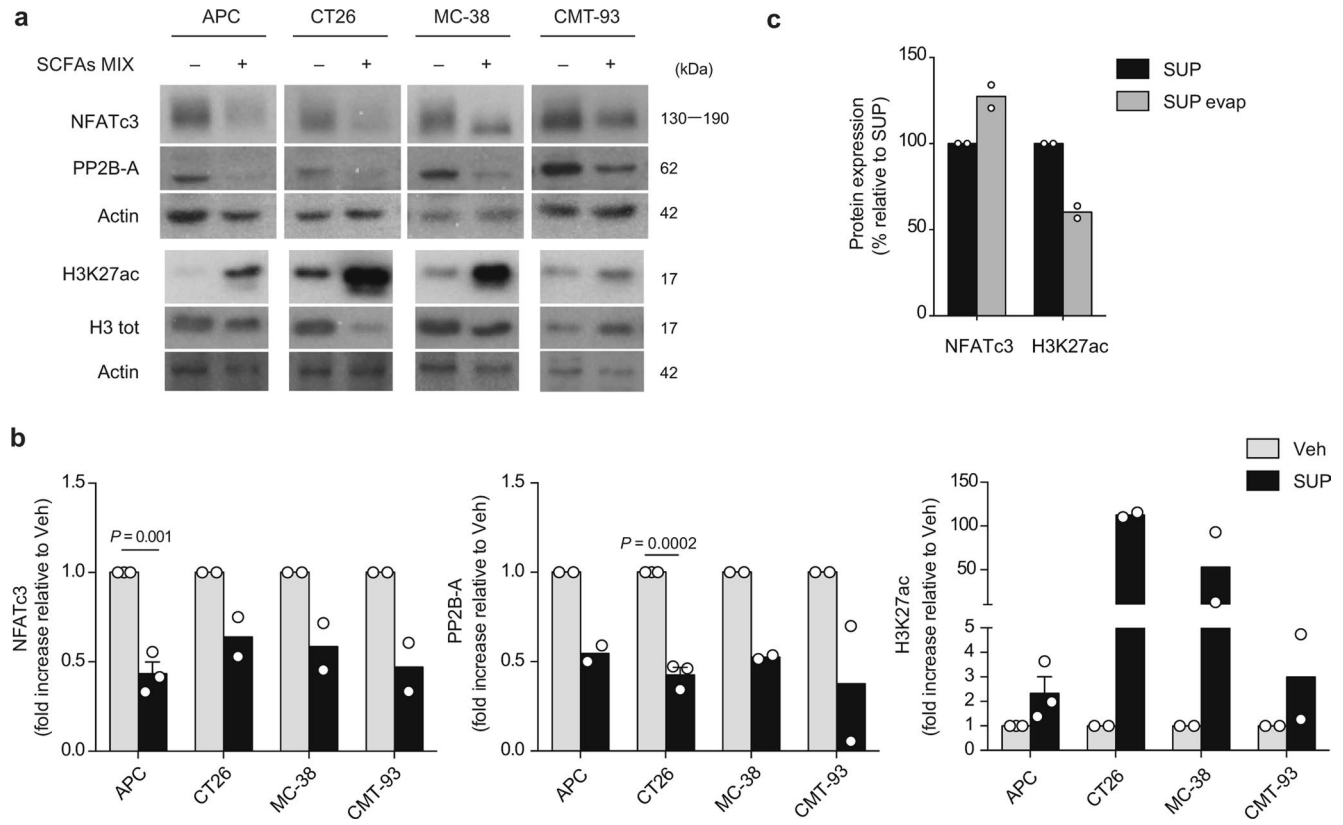

Extended Data Fig. 5 | SCFAs and *F. PB1* spent medium (SUP) increase histone H3 acetylation and reduce NFATc3-calcineurin pathway *in vitro* on mouse intestinal tumour cell lines. a, Representative WB showing H3K27 acetylation, PP2B-A and NFATc3 in cell lines treated (+) or not (-) with a mix of SCFAs. Three independent experiments were performed with consistent results. **b**, Densitometric quantification of WB in Fig. 4d showing NFATc3 and PP2B-A (normalized to actin) and H3K27 acetylation (normalized to vinculin). Two or three independent experiments were performed with consistent results (n = 2 or n = 3 biologically independent experiments). Data are represented as means ± s.e.m. and *P* values were determined by two-tailed unpaired Student's *t*-test. **c**, Densitometric quantification of WB in Fig. 4e showing NFATc3 (normalized to vinculin) and H3K27 acetylation (normalized to H3 tot). To calculate the protein expression induced by SUP evap as a percentage, the densitometric value of SUP was assumed to be 100%. Data from two independent WB (n = 2 biologically independent experiments).

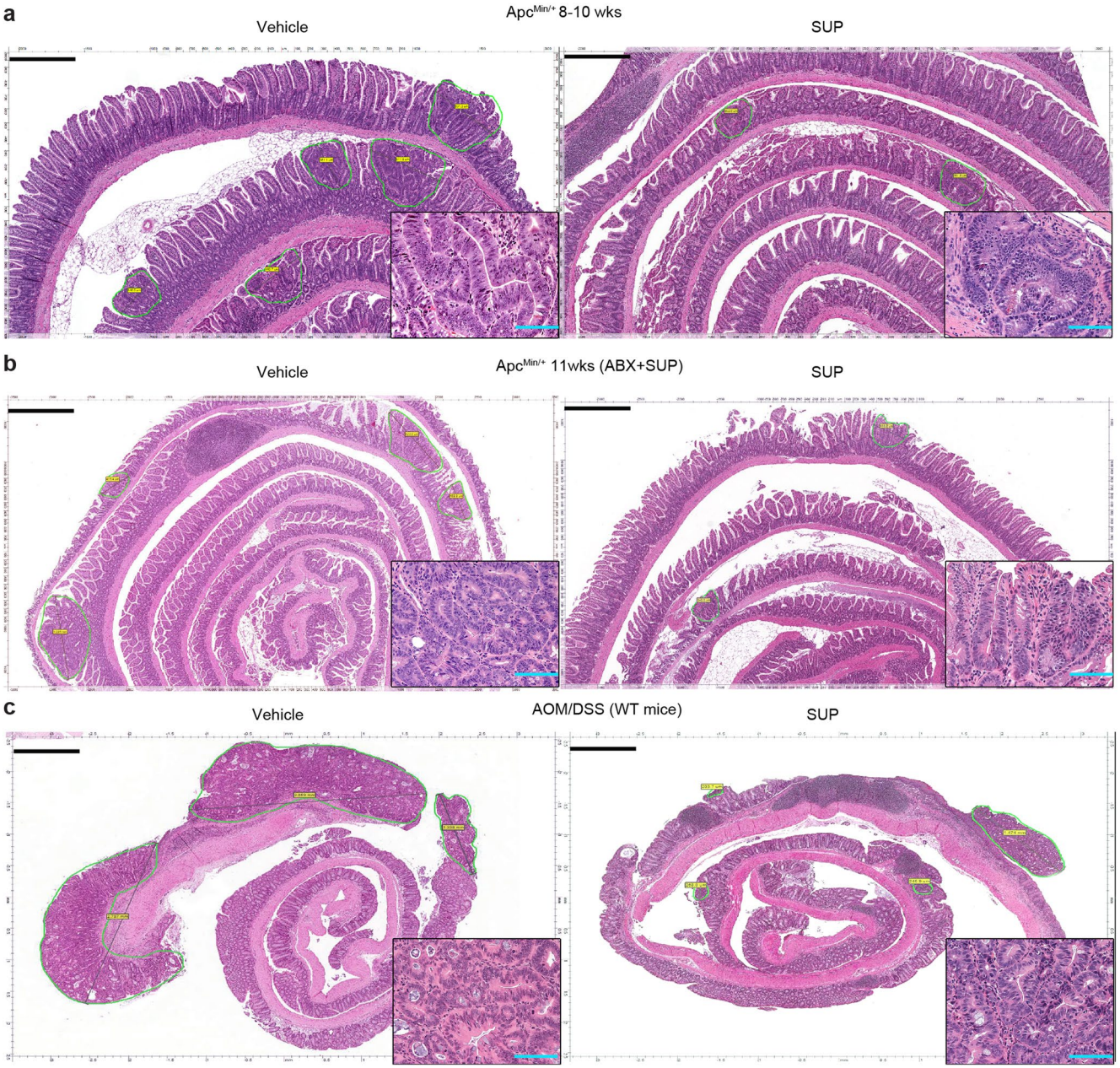

Extended Data Fig. 6 | Effect of *F.* PB1 spent medium (SUP) in tumourigenesis. a-**c**, Representative histologies from ileal and colon sections of $Apc^{Min/+}$mice (**a**,Veh n = 13; SUP n =11 mice/group; **b**,Veh n = 6; SUP n =7 mice/group) and AOM and DSS treated WT mice (**c**,Veh n = 5; SUP n = 6 mice/group) treated with vehicle or *F.* PB1 SUP. Sections stained for H&E from FFPE blocks of swiss roll of small (**a**, 5X magnification, scale bars 500 μm; **b**, 3X magnification, scale bars 750 μm) and large (**c**, 2X magnification, scale bars 900 μm) bowel and treated as indicated by labels. Slides were scanned by Aperio Scanscope and digital images were obtained. Dysplastic lesions were selected and measured. In the lower right high power insert, a detail of dysplastic glands (200X magnification, blue scale bars 100 μm).

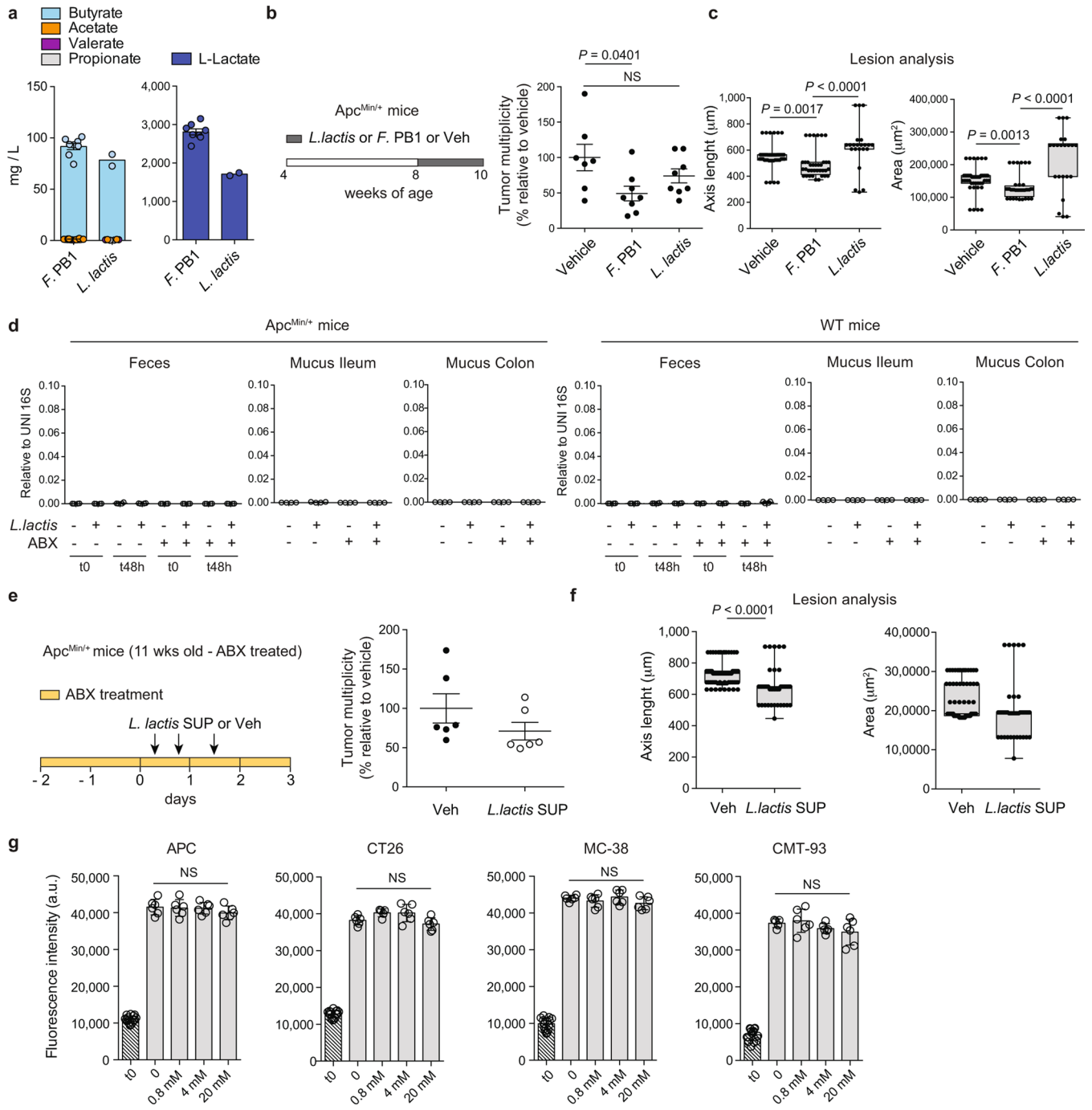

Extended Data Fig. 7 | *L. lactis* does not colonize the mouse gut but its spent medium (SUP) has anti-tumourigenic effect *in vivo*. **a**, Quantification of SCFAs in SUP of *F.* PB1 and *L. lactis* by UPLC–HR–MS. Data from 2 or 6 independent experiments (*L.lactis* SUP n = 2; *F.* PB1 SUP n = 6 biologically independent experiments). **b**,**c**, Apc$^{Min/+}$ mice received vehicle (Veh, n = 7 mice/group), *F.* PB1 or *L. lactis* (n = 8 mice/group) from week 8 to 10. **b**, Tumour multiplicity in the small intestine normalized to vehicle-treated Apc$^{Min/+}$ mice. **c**, Area and maximum diameter (axis lenght) of ileal dysplastic lesions normalized to the total number of lesions per mouse. Box plots show the interquartile range, median value and whiskers min to max. **d**, qPCR of *L. lactis* abundance normalized to panbacterial primers targeting the 16S rRNA gene (UNI 16S) in bacterial DNA extracted from faeces (both at time 0 and 48h after last gavage) and mucus from the ileum and colon of WT and Apc$^{Min/+}$ mice pretreated or not with antibiotics (ABX) and then monocolonized with *L. lactis* (n = 4 mice/group). **e**,**f**, 11 weeks old Apc$^{Min/+}$ mice treated with broths not fermented (Veh) or fermented by *L. lactis* (SUP) in the presence of ABX (n = 6 mice/group). **e**, tumour multiplicity in the small intestine normalized to vehicle-treated Apc$^{Min/+}$ mice. **f**, Area and maximum diameter of ileal dysplastic lesions normalized to the total number lesions per mouse. Box plots show the interquartile range, median value and whiskers min to max. **g**, Cell proliferation assay on mouse CRC cell lines treated or not with sodium lactate at different concentrations for 48h. t0 is the signal from cells at the time of stimulation. Two independent experiments were performed with consistent results. Data presented as means ± s.d. of a representative experiment (n = 6 biologically independent samples). *P* values were determined by two-tailed unpaired Mann-Whitney U test (**e**,**f**), one-way ANOVA with Bonferroni post-test (**b**,**g**) or Kruskal-Wallis test with Dunn post-test (**c**,**d**). Data are presented as means ± s.e.m. in **a**-**f**.

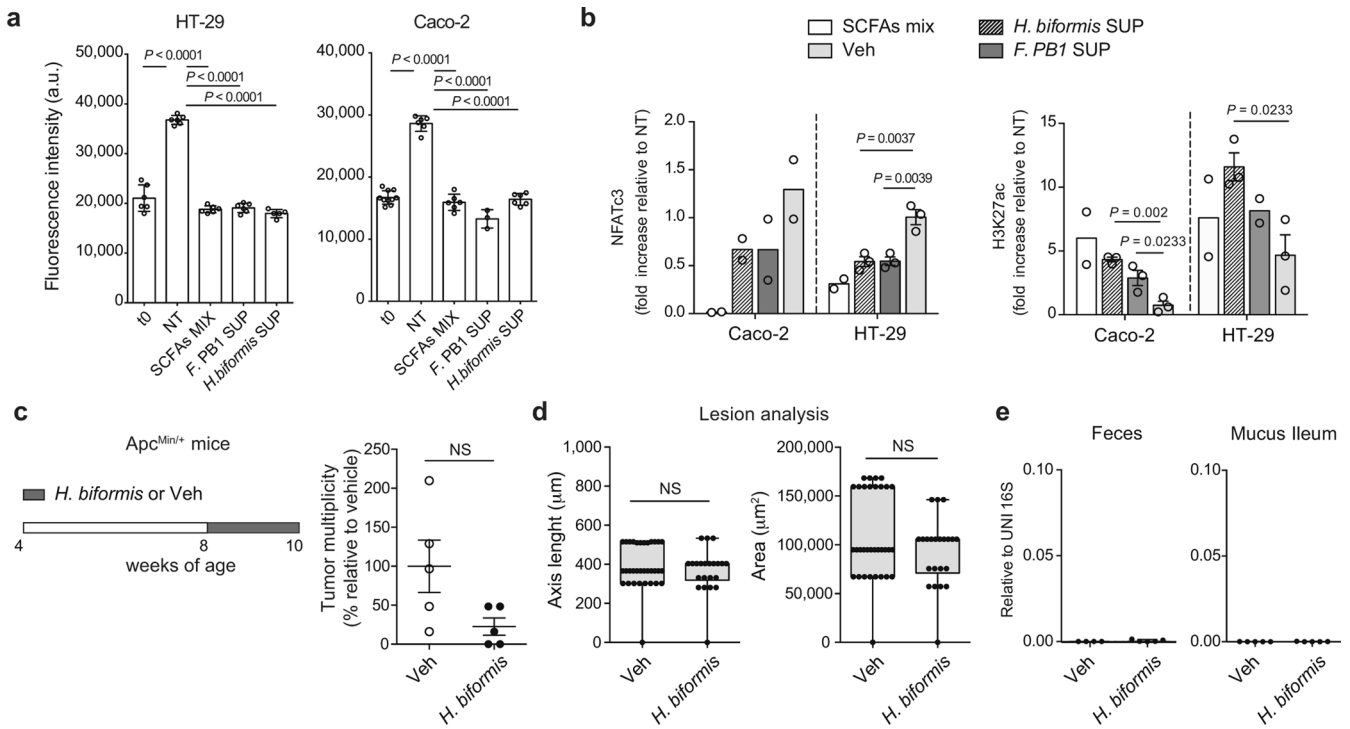

Extended Data Fig. 8 | *H. biformis* does not colonize the mouse gut but its spent medium (SUP) increases histone H3 acetylation, reduces NFATc3 activation and proliferation *in vitro* on human colorectal cancer cell lines. a, Cell proliferation assay on human CRC cell lines treated or not (NT) with broth fermented by *F.* PB1 (*F.* PB1 SUP) or by *H. biformis* (*H. biformis* SUP) and with a mix of SCFAs as a control. t0 is the signal from cells at the time of stimulation. Two independent experiments were performed with consistent results. Data are presented as means ± s.d. of a representative experiment (n = 6 biologically independent samples). **b**, Densitometric quantification of WB in Fig. 6e showing NFATc3 and H3K27 acetylation (normalized to vinculin). Two or three independent experiments were performed with consistent results (n = 2 or n = 3 biologically independent experiments). **c**-**e**, $Apc^{Min/+}$ mice received vehicle (Veh) or *H. biformis* from week 8 to 10 (n = 5 mice/group). **c**, tumour multiplicity in the small intestine normalized to vehicle-treated $Apc^{Min/+}$ mice. **d**, Area and maximum diameter (axis lenght) of ileal dysplastic lesions normalized to the total number of lesions per mouse. Box plots show the interquartile range, median value and whiskers min to max. **e**, qPCR of *H. biformis* abundance normalized to panbacterial primers targeting the 16S rRNA gene (UNI 16S) in bacterial DNA extracted from faeces and mucus from the ileum. *P* values were determined by one-way ANOVA using Bonferroni (**a**) or Tukey (**b**, NFATc3 HT29 and H3K27 Caco2) post-test, by two-tailed unpaired Student's *t*-test (**b**, H3K27 HT29) or by two-tailed Mann-Whitney U test (**c**-**e**). Data are represented as means ± s.e.m. in **b**-**e**.

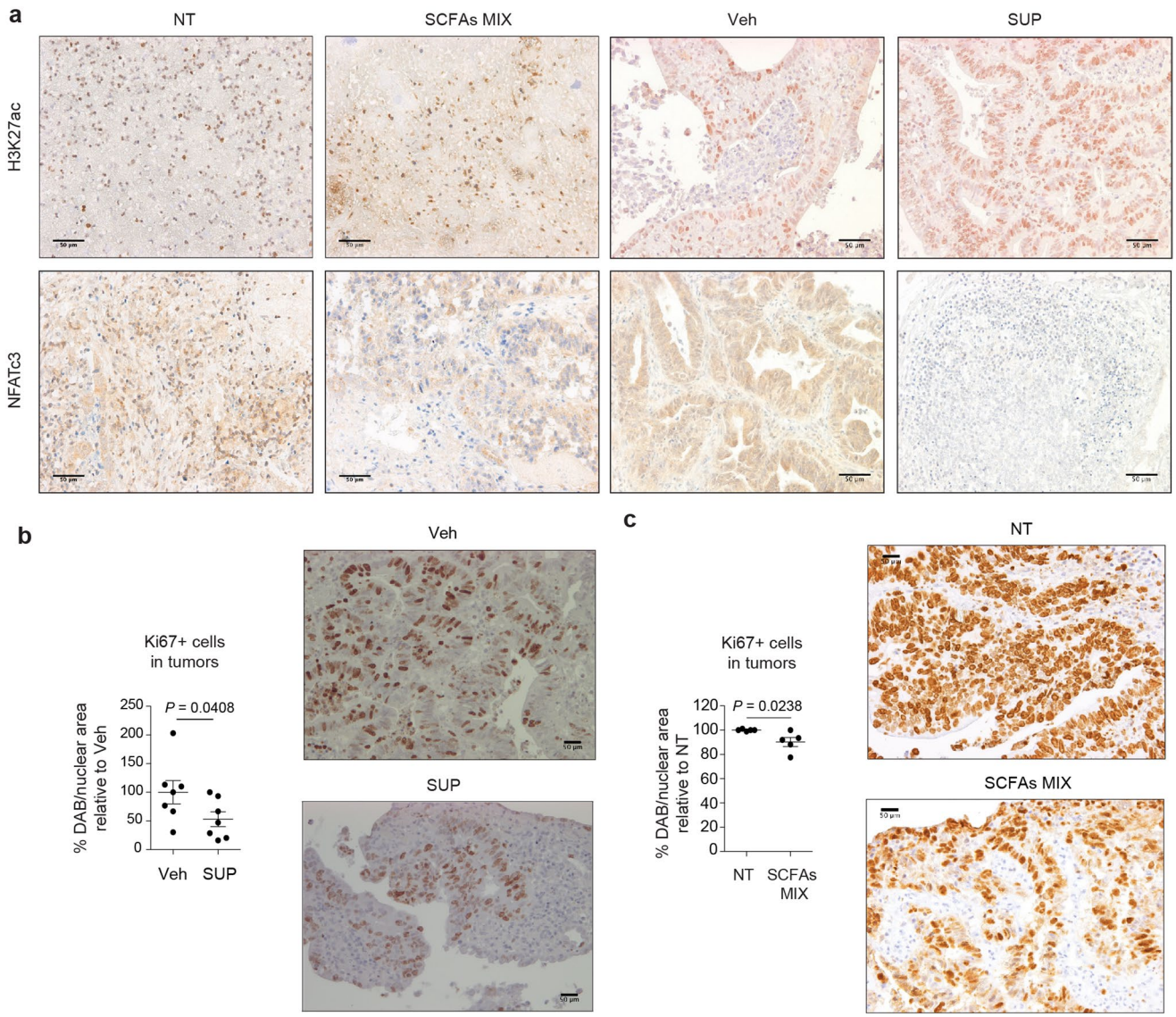

Extended Data Fig. 9 | Treatments with SCFAs or *F. PB1* spent medium (SUP) increase histone H3 acetylation, reduce NFATc3 activation and proliferation in human CRC samples. a-c, Human colon tumour samples (hCRC) incubated *ex vivo* with broth fermented with *F. PB1* (SUP) or non-fermented (Veh); with medium alone (NT) or with SCFAs MIX. **a**, Representative immunohistochemistry of one out of three independent experiments of H3K27 acetylation and NFATc3 expression. Scale bars, 50 µm. **b**,**c**, Representative images of ileal dysplastic lesions stained with Ki67. Scale bars, 50 µm. Three independent experiments were performed with consistent results. Dot plots show the percentage of Ki67 positive cells relative to vehicle (**b**) or to NT (**c**). Data from three independent experiments (**b**, n = 7; **c**, n = 5 biologically independent samples), are represented as means ± s.e.m. and *P* values were determined by two-tailed unpaired Mann-Whitney U test.

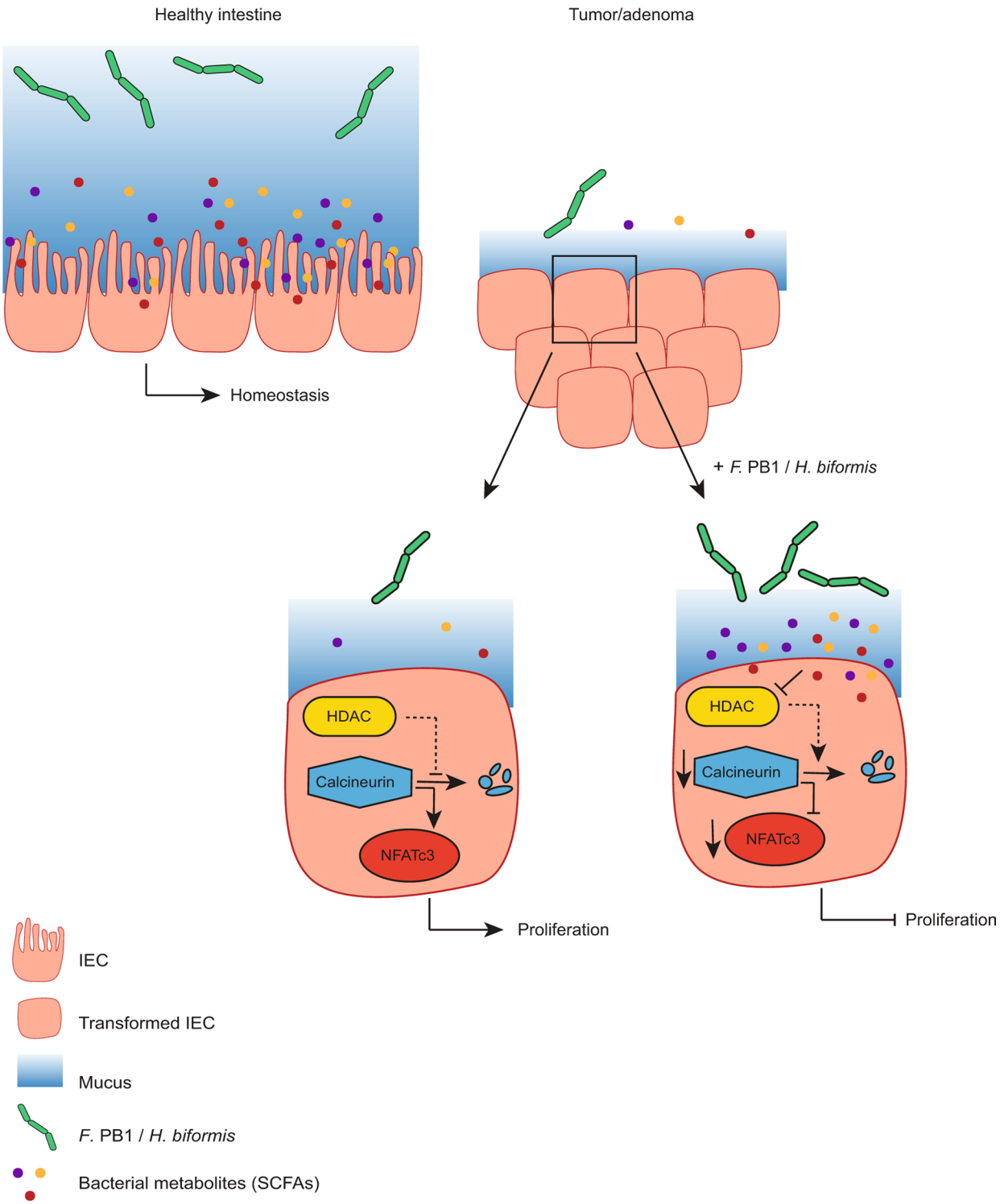

Extended Data Fig. 10 | Model. Upon intestinal tumourigenesis selectively some bacterial species do not expand, due to different mucus composition or to competition with other bacteria and their corresponding metabolites. If these bacterial species are reintroduced, they induce the release of SCFAs. *F.* PB1 or *H. biformis* metabolic products act as HDAC inhibitors in the adenomas inducing an increase in acetylation and downmodulation of the calcineurin-NFATc3 pathway, which is involved in cell proliferation.

nature research

Corresponding author(s): Maria Rescigno NMICROBIOL-18122604B

Last updated by author(s): Oct 6, 2019

Reporting Summary

Nature Research wishes to improve the reproducibility of the work that we publish. This form provides structure for consistency and transparency in reporting. For further information on Nature Research policies, see Authors & Referees and the Editorial Policy Checklist.

Statistics

For all statistical analyses, confirm that the following items are present in the figure legend, table legend, main text, or Methods section.

n/a	Confirmed	
☐	☒	The exact sample size (*n*) for each experimental group/condition, given as a discrete number and unit of measurement
☐	☒	A statement on whether measurements were taken from distinct samples or whether the same sample was measured repeatedly
☐	☒	The statistical test(s) used AND whether they are one- or two-sided *Only common tests should be described solely by name; describe more complex techniques in the Methods section.*
☒	☐	A description of all covariates tested
☐	☒	A description of any assumptions or corrections, such as tests of normality and adjustment for multiple comparisons
☐	☒	A full description of the statistical parameters including central tendency (e.g. means) or other basic estimates (e.g. regression coefficient) AND variation (e.g. standard deviation) or associated estimates of uncertainty (e.g. confidence intervals)
☒	☐	For null hypothesis testing, the test statistic (e.g. *F*, *t*, *r*) with confidence intervals, effect sizes, degrees of freedom and *P* value noted *Give P values as exact values whenever suitable.*
☒	☐	For Bayesian analysis, information on the choice of priors and Markov chain Monte Carlo settings
☒	☐	For hierarchical and complex designs, identification of the appropriate level for tests and full reporting of outcomes
☒	☐	Estimates of effect sizes (e.g. Cohen's *d*, Pearson's *r*), indicating how they were calculated

Our web collection on statistics for biologists contains articles on many of the points above.

Software and code

Policy information about availability of computer code

Data collection	FACS Diva (BD, v6.2 and v8.0.1), Leica Application Suite X (v3.5.5.19976), Real-Time PCR System Software (Applied Biosystems, v.1.0), Aperio ImageScope Software (Leica Biosystems v12.3.3.5048), Xcalibur v4.0, PEAR (v0.9.6), Usearch (v6.0.307), Bowtie2 (v2.3.4.1), Tango (v1.0)
Data analysis	Prism (GraphPad software, v6.01b), Excel (Microsoft Office, v17.7.7), FlowJo (FlowJo, v10.5.3), Fiji (ImageJ v2.0.0-rc-69/1.52n), PhyloPhlAn2 (v0.40), curatedMetagenomicData (v1.14.1), MetaPhlAn2 (v2.7.8), DESeq2 (v3.2), Vegan (v2.5.6), LEfSe (v1.0.7), ggplot2 (v3.2.1)

For manuscripts utilizing custom algorithms or software that are central to the research but not yet described in published literature, software must be made available to editors/reviewers. We strongly encourage code deposition in a community repository (e.g. GitHub). See the Nature Research guidelines for submitting code & software for further information.

Data

Policy information about availability of data

All manuscripts must include a data availability statement. This statement should provide the following information, where applicable:

- Accession codes, unique identifiers, or web links for publicly available datasets
- A list of figures that have associated raw data
- A description of any restrictions on data availability

All relevant data have been included in the paper. Source Data for the figures and extended data figures are provided in the online version of the paper. Raw sequencing data and metadata associated to samples are available online at https://www.ncbi.nlm.nih.gov/bioproject/PRJNA564752.

Field-specific reporting

Please select the one below that is the best fit for your research. If you are not sure, read the appropriate sections before making your selection.

☒ Life sciences ☐ Behavioural & social sciences ☐ Ecological, evolutionary & environmental sciences

For a reference copy of the document with all sections, see nature.com/documents/nr-reporting-summary-flat.pdf

Life sciences study design

All studies must disclose on these points even when the disclosure is negative.

Sample size	Sample size was chosen taking in consideration the means of the target values between the experimental group and the control group, the standard error and the statistical analysis used. For animal studies, sample size was defined on the basis of past experience with the models, to detect differences of 20% or greater between the groups (10% significance level and 80% power). For ethical reasons, the minimum number of animals necessary to achieve the scientific objectives was used.
Data exclusions	Grubb's test was applied to exclude outliers.
Replication	To verify the reproducibility of the experimental findings, all the experiments were performed at least two/three times/each (reported in the figure legends), giving us similar results.
Randomization	Animals were allocated randomly to each treatment group. Different treatment groups were processed identically, and animals in different treatment groups were exposed to the same environment.
Blinding	In IHC and IF analyses, the investigators were unaware of the experimental groups.

Reporting for specific materials, systems and methods

We require information from authors about some types of materials, experimental systems and methods used in many studies. Here, indicate whether each material, system or method listed is relevant to your study. If you are not sure if a list item applies to your research, read the appropriate section before selecting a response.

Materials & experimental systems

n/a	Involved in the study
☐	☒ Antibodies
☐	☒ Eukaryotic cell lines
☒	☐ Palaeontology
☐	☒ Animals and other organisms
☐	☒ Human research participants
☒	☐ Clinical data

Methods

n/a	Involved in the study
☒	☐ ChIP-seq
☐	☒ Flow cytometry
☒	☐ MRI-based neuroimaging

Antibodies

Antibodies used

FACS antibodies: CD16/32 – unconjugated (clone93, 14-0161-82, Ebiosciences; 1:50); CD45.2-V450 (clone 104, 560697, BD biosciences, 1:200); CD3-PE-Cy7 (clone 145-2C11, 552774, BD biosciences, 1:200); CD4-FITC (clone RM4-5, 553047, BD biosciences, 1:200); CD25-APC-Cy7 (clone PC61, 102026, Biolegend, 1:200); FoxP3-PE (clone FJK-16s, 12-5773-82, Ebiosciences, 1:100); Helios-Alexa-fluor647 (clone 22F6, 51-9883-82, Ebiosciences, 1:100); IL17-PE (clone TC11-18H10, 559502, BD biosciences, 1:100); IFNγ-APC (clone XMG1.2,554413, BD biosciences, 1:100); Ly6G-APC (clone 1A8, 560599, BD biosciences, 1:200); Ly6G-APC-Cy7 (clone 1A8, 127624, Biolegend, 1:200); Ly6C-FITC (clone AL-21, 553104, BD biosciences, 1:200); F4/80-APC (clone BM8,17-4801-82, Ebiosciences, 1:200); CD11b-PerCP- Cy5.5 (clone M1/70, 550993, BD Biosciences, 1:200); CD11c-BV650 (clone N418, 117339, Biolegend, 1:200); Fixable viability stain510 (564406, BD Biosciences, 1:1000). For flow gating we used florescence minus one (FMO) controls.

Western blot antibodies: anti-PP2B-A (cat. n°sc-9070, clone H-209, Santa Cruz Biotechnology, 1:1000); anti-NFATc3 polyclonal (clone M-75, cat. n°sc-8321, lot H2010, Santa Cruz Biotechnology, 1:1000); anti-NFATc3 monoclonal (clone F-1, cat. n°sc-8405, lot D1117, Santa Cruz Biotechnology, 1:1000); anti-Histone H3 acetyl K27 (cat. n°ab4729, lot. GR183922-1, abcam, 1:1000); anti-Histone H3 (cat. n°ab1791, abcam, 1:1000); anti-actin (clone AC-40, cat. n°A4700, Sigma, 1:1000); anti-vinculin (clone hVIN-1, cat. n°V9264, Sigma, 1:10000); anti-Muc1 (clone F-19, cat. n°sc-6826, lot. K0512, Santa Cruz Biotechnology, 1:200); anti-Muc13 (cat. n°ab124654, lot. GR119772-30, abcam, 1:1000); anti-Muc20 (cat. n° PA5-50238, lot. SK2477888, Thermofisher, 1:1000); secondary antibodies goat anti-rabbit-HRP (cat. n°170-6515, Bio-Rad, 1:10000); goat anti-mouse-HRP (cat. n°170-6516, Bio-Rad, 1:10000); rabbit anti-goat (cat. n°P0449, lot. 20036798, DAKO, 1:2000).

Immunofluorescence: primary antibody anti-Muc1 (Rabbit polyclonal antibody, clone aa 474-630, cat. n°LS-C343984, lot. 72576, LifeSpan Bioscience, 1:100); secondary antibody donkey anti-rabbit-cy3 (cat. n° 711165153, lot. 130437, Jackson Immuno

	research, 1:300). Immunohistochemistry: anti-Ki67 antibody (ab15580, abcam, 1:200); anti-NFATc3 polyclonal (clone M-75, cat. n°sc-8321, lot H2010,Santa Cruz Biotechnology, 1:200); anti-NFATc3 monoclonal (clone F-1, cat. n°sc-8405, lot D1117, Santa Cruz Biotechnology, 1:200); anti Histone H3 acetyl K27 (cat. n°ab4729, lot. GR183922-1, abcam, 1:500 for human and 1:800 for mouse tissues).
Validation	For FACS analysis, after neutralization of unspecific binding with αCD16/CD32 (clone 93, EBioscence), single-cell suspensions were stained with specific mAb (primary antibodies directly conjugated) to assess the phenotype. To validate IHC antibodies, positive and negative controls were incubated with and without primary antibody. Reactivity of primary antibodies for WB and IF was verified adding a positive control in each experiment. Specificity of secondary antibody for IF was verified using only secondary antibody as negative control.

Eukaryotic cell lines

Policy information about cell lines

Cell line source(s)	CT26, HT-29 and Caco-2 cell lines were purchased from the American Type Culture Collection (ATCC). CMT-93 cell line is a kind gift of Dr. David Artis (Cornell University, NY, USA). MC-38 cell line is a kind gift of Dr Carsten Krieg (Zurich University, Switzerland). APC cell line was derived from ApcMin/+ small intestinal adenomas by mechanical disruption.
Authentication	Cell lines were purchased from the American Type Culture Collection (ATCC) and no other authentication method was performed. In APC cell line, derived from ApcMin/+ small intestinal adenomas, the loss of heterozygosity (loss of the WT allele and presence of the Min allele) was checked by TaqMan assay.
Mycoplasma contamination	All cell lines were tested to exclude mycoplasma contamination.
Commonly misidentified lines (See ICLAC register)	No commonly misidentified cell lines were used.

Animals and other organisms

Policy information about studies involving animals; ARRIVE guidelines recommended for reporting animal research

Laboratory animals	This study employed both male and female mice (Mus musculus) of the following strains as model organisms: C57BL6/J ; C57BL6/J-ApcMin/J; Germ-free ICR. 6 weeks old C57BL6/J mice were purchased from Harlan Laboratories. C57BL6/J457 ApcMin/J (referred to as ApcMin/+) were maintained as inbred strain in our animal facility. For experiments where ApcMin/+ were employed, wild type littermates born from the same mothers of experimental mice were used as controls. All mice were maintained in microisolator cages in specific pathogen-free (SPF) animal facility. Germ-free ICR male mice were maintained in the isolators at RIKEN IMS (Yokohama, Japan).
Wild animals	The study did not involve wild animals.
Field-collected samples	The study did not involve samples collected from the field.
Ethics oversight	Experiments were performed in accordance with the guidelines established in the Principles of Laboratory Animal Care (directive 86/609/EEC) and approved by the Italian Ministry of Health (n. 139/15).

Note that full information on the approval of the study protocol must also be provided in the manuscript.

Human research participants

Policy information about studies involving human research participants

Population characteristics	Colonic human specimens were obtained from patients diagnosed with colon cancer and undergoing surgery at IEO. Inclusion criteria were newly diagnosed CRC patients (stage: I to III), aged between 35-70 years old, performance status 0-1 based on the Eastern Cooperative Oncology Group (E 948 COG). Exclusion criteria were a personal history of malabsorption syndrome or any chronic inflammatory bowel disease, or subjects with hereditary syndrome (such as FAP HNPCC) and use of antibiotics in the previous four weeks.
Recruitment	All patients given written informed consent and were enrolled in institutional protocol approved by IEO's ethical committee. Human biological samples were sourced ethically and their research use was in accord with the terms of the informed consent provided. Case selection was therefore independent and blinded to baseline characteristics, treatments received, clinical outcome and molecular characterization to reduce any potential self-selection bias.
Ethics oversight	The protocol was approved by the IEO's ethical committee.

Note that full information on the approval of the study protocol must also be provided in the manuscript.

Flow Cytometry

Plots

Confirm that:

☐ The axis labels state the marker and fluorochrome used (e.g. CD4-FITC).

☐ The axis scales are clearly visible. Include numbers along axes only for bottom left plot of group (a 'group' is an analysis of identical markers).

☐ All plots are contour plots with outliers or pseudocolor plots.

☒ A numerical value for number of cells or percentage (with statistics) is provided.

Methodology

Sample preparation	Peripheral blood was sampled in heparin and red blood cells were lysed. Small intestinal and colonic lamina propria (LP) lymphocytes were isolated incubating intestinal chunks PBS 5% FCS 1,5 mM EDTA 1mM DTT at 37°C for 15 min to remove epithelial cells. LP cells were mechanically isolated in RPMI 5% FCS with GentleMACS dissociator.
Instrument	FACSCanto II and Fortessa (BD Bioscience)
Software	FlowJo (Treestar, v10.5.3)
Cell population abundance	*Describe the abundance of the relevant cell populations within post-sort fractions, providing details on the purity of the samples and how it was determined.*
Gating strategy	Fig. 3a and Extended Data 3a-e: gate on SSC-A/FSC-A, gate on FSC-A/FCS-H for singlets, gate on CD45+ viability dye-, gate on CD3+CD4+. Tregs gated as FoxP3+ CD25+. Within FoxP3+ CD25+ gated Helios+ events. For Th1/Th17 after gating on CD3+ CD4+ quadrant gate on IL17 and IFNγ. Fig. 3b and Extended Data 3h: gate on SSC-A/FSC-A, gate on FSC-A/FCS-H for singlets, gate on CD45+CD3- population. Neutrophils were gated as CD11b+ Ly6G+, inflammatory monocytes were gated as CD11b+ Ly6Chi. Extended Data 3f,g: gate on SSC-A/FSC-A, gate on FSC-A/FSC-H for singlets, gate on CD45+ viability dye- CD3- population. Neutrophils were gated as CD11b+Ly6G+. Within the NOT(neutrophils) events we gated the macrophages as CD11b+ F4/80+. Within the NOT(neutrophils)NOT(macrophages) events we gated the myeloid dendritic cell population as CD11c+CD11b+ and the Inflammatory monocytes population as CD11c-CD11b+Ly6Chi.

☒ Tick this box to confirm that a figure exemplifying the gating strategy is provided in the Supplementary Information.